Inorg. Chem. **2002**, *41*, 6673–6687

Influence of Electronic and Structural Effects on the Oxidative Behavior of Nickel Porphyrins

Karl M. Kadish,*,† Min Lin,† Eric Van Caemelbecke,†,‡ Guido De Stefano,† Craig J. Medforth,*,§,∥ Daniel J. Nurco,§ Nora Y. Nelson,§ Bénédicte Krattinger,§ Cinzia M. Muzzi,§ Laurent Jaquinod,§ Yang Xu,§ David C. Shyr,§ Kevin M. Smith,*,§ and John A. Shelnutt⊥,∥

Department of Chemistry, University of Houston, Texas 77204-5641, Department of Chemistry, Houston Baptist University, Texas 77074-3298, Department of Chemistry, University of California, Davis, California 95616-5295, Biomolecular Materials and Interfaces Department, Sandia National Laboratories, Albuquerque, New Mexico 87185, and Department of Chemistry, University of Georgia, Athens, Georgia 30602-2556

Received January 24, 2002

With the aim of better understanding the electronic and structural factors which govern electron-transfer processes in porphyrins, the electrochemistry of 29 nickel(II) porphyrins has been examined in dichloromethane containing either 0.1 M tetra-*n*-butylammonium perchlorate (TBAP) or tetra-*n*-butylammonium hexafluorophosphate ($TBAPF_6$) as supporting electrolyte. Half-wave potentials for the first oxidation and first reduction are only weakly dependent on the supporting electrolyte, but $E_{1/2}$ for the second oxidation varies considerably with the type of supporting electrolyte. $E_{1/2}$ values for the first reduction to give a porphyrin π-anion radical are effected in large part by the electronic properties of the porphyrin macrocycle substituents, while half-wave potentials for the first oxidation to give a π-cation radical are affected by the substituents as well as by nonplanar deformations of the porphyrin macrocycle. The potential difference between the first and second oxidations ($\Delta|Ox_2 - Ox_1|$) is highly variable among the 29 investigated compounds and ranges from 0 mV (two overlapped oxidations) to 460 mV depending on the macrocycle substituents and the anion of the supporting electrolyte. The magnitude of $\Delta|Ox_2 - Ox_1|$ is generally smaller for compounds with very electron-withdrawing substituents and when TBAP is used as the supporting electrolyte. This behavior is best explained in terms of differences in the binding strengths of anions from the supporting electrolyte (ClO_4^- or PF_6^-) to the doubly oxidized species. A closer analysis suggests two factors which are important in modulating $\Delta|Ox_2 - Ox_1|$ and thus the binding affinity of the anion to the porphyrin dication. One is the type of π-cation radical (a proxy for the charge distribution in the dication), and the other is the conformation of the porphyrin macrocycle (either planar or nonplanar). These findings imply that the redox behavior of porphyrins can be selectively tuned to display separate or overlapped oxidation processes.

Introduction

Over the past three decades, nickel(II) porphyrins have been extensively studied as to their spectroscopic and redox properties and a detailed review of their electrochemistry in nonaqueous media has recently appeared in the literature.[1] Nickel porphyrins can be oxidized in up to three one-electron-transfer steps,[2] depending upon the solvent, although the third oxidation is not always observed. They are also typically reduced in two one-electron-transfer steps, although some Ni(II) porphyrins with highly electron-withdrawing groups can be reduced by a total of three electrons.[3] In most

* To whom correspondence should be addressed. E-mail: kkadish@uh.edu (K.M.K).
† University of Houston.
‡ Houston Baptist University.
§ University of California.
∥ Sandia National Laboratories.
⊥ University of New Mexico.

(1) Kadish, K. M.; Van Caemelbecke, E.; Royal, G. In *The Porphyrin Handbook*; Kadish, K. M., Smith, K. M., Guilard, R., Eds.; Academic Press: Boston, 2000; Vol. 8, p 1.
(2) Kadish, K. M.; Caemelbecke, E. V.; Boulas, P.; D'Souza, F.; Vogel, E.; Kisters, M.; Medforth, C. J.; Smith, K. M. *Inorg. Chem.* **1993**, *32*, 4177.
(3) Ozette, K.; Leduc, P.; Palacio, M.; Bartoli, J. F.; Barkigia, K. M.; Fajer, J.; Battioni, P.; Mansuy, D. *J. Am. Chem. Soc.* **1997**, *119*, 6442.

10.1021/ic0200702 CCC: $22.00
Published on Web 11/19/2002

cases, the initial oxidations and reductions involve the porphyrin π-system, but examples where the first electron is removed or added to the central metal ion to give a nickel(III) species[4−6] or a nickel(I) species[7−9] are well documented in the literature.

The goal of the present study is to understand in more detail how the electronic properties of the peripheral substituents of a nickel porphyrin and the structural properties of the porphyrin macrocycle influence the oxidative behavior of the compound, and specifically how they are related to the electron-transfer mechanism. A previous electrochemical study of six nickel(II) porphyrins[10] showed that the absolute potential separation between the first two oxidations, $\Delta|Ox_2 - Ox_1|$, varied as a function of the type of supporting electrolyte and the substituents on the porphyrin macrocycle. In some cases, two one-electron oxidations were seen upon going from the neutral compound to the dication, and in other cases the two one-electron oxidations were overlapped. For example, depending upon the compound, $\Delta|Ox_2 - Ox_1|$ varied from 480 to 0 mV in dichloromethane solutions containing 0.1 M tetra-*n*-butylammonium perchlorate (TBAP).[10] However, for the same compounds in dichloromethane solutions with tetra-*n*-butylammonium hexafluorophosphate ($TBAPF_6$), $\Delta|Ox_2 - Ox_1|$ varied from 510 to 240 mV and none of the oxidations were overlapped. We wished to examine nickel porphyrins with a much larger range of substituents to determine the factors responsible for overlap of the oxidations. Such a study is discussed in this paper. The first section under Results and Discussion describes the electrochemical behavior of nickel porphyrins **1**−**29** (see Figure 1 and Table 1) in dichloromethane containing two different supporting electrolytes [0.1 M TBAP or 0.1 M $TBAPF_6$]. The second section under Results and Discussion (Structural Studies) details the structures of the nickel porphyrins as determined using X-ray crystallography and molecular mechanics calculations. Porphyrins **1**−**29** can be divided into derivatives with T(aryl)P, T(alkyl)P, T(X)OEP, Br_8T(aryl)P, and D(aryl)P substituent patterns (see Figure 1). These groups are shown to encompass significant variations in the type of nonplanar deformation of the porphyrin macrocycle induced by the peripheral substituents in addition to the expected electronic effects of the substituents. In the last section under Results and Discussion, the data obtained from the electrochemical and structural studies are used to analyze the dependence of the half-wave potentials on the electronic properties of the substituents, the structural properties of the porphyrin, and the type of supporting electrolyte.

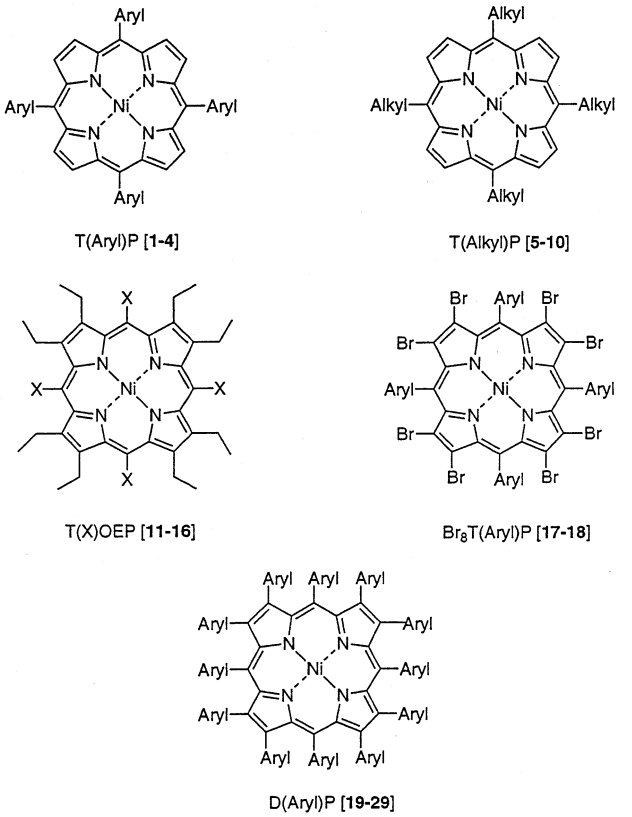

Figure 1. Structures of the porphyrins investigated.

Table 1. List of the Nickel Porphyrins Investigated[a]

compd	group	macrocycle (P)	meso substituents	β substituents
1	T(aryl)P	TPP	Ph	H
2		T(4-Cl-P)P	4-Cl-Ph	H
3		T(4-Et_2N-P)P	4-N$(Et)_2$-Ph	H
4		F_{20}TPP	C_6F_5	H
5	T(alkyl)P	T(^{t}Bu)P	^{t}Bu	H
6		T(C_3F_7)P	$CF_2CF_2CF_3$	H
7		T(^{i}Pr)P	^{i}Pr	H
8		T(Me)P	Me	H
9		T(Et)P	Et	H
10		T(Pr)P	Pr	H
11	T(X)OEP	T(Bz)OEP	OCOPh	Et
12		OET(3-Th)P	3-thienyl	Et
13		OETPP	Ph	Et
14		OETNP	NO_2	Et
15		F_{20}OETPP	C_6F_5	Et
16		TC6TPP	Ph	$(CH_2)_4$
17	Br_8T(aryl)P	Br_8TPP	Ph	Br
18		Br_8F_{20}TPP	C_6F_5	Br
19	D(aryl)P	DPP	Ph	Ph
20		F_4DPP	4-F-Ph	Ph
21		F_8DPP	Ph	4-F-Ph
22		F_{12}DPP	4-F-Ph	4-F-Ph
23		$(OMe)_{20}$DPP	3,4,5-tri-OMe-Ph	4-OMe-Ph
24		OPT(3-Th)P	3-thienyl	Ph
25		F_8DPP (meso)	2,6-di-F-Ph	Ph
26		F_{20}DPP	C_6F_5	Ph
27		F_{28}DPP	C_6F_5	4-F-Ph
28		F_{36}DPP	C_6F_5	3,5-di-F-Ph
29		T(4-NO_2-P)OPP	4-NO_2-Ph	Ph

[a] Schematic representations of the different groups of macrocycles are shown in Figure 1.

Results and Discussion

I. Electrochemical Studies. Reversible half-wave potentials for the reduction and oxidation of the 29 nickel(II) por-

(4) Seth, J.; Palaniappan, V.; Bocian, D. F. *Inorg. Chem.* **1995**, *34*, 2201.
(5) Connick, P. A.; Macor, K. A. *Inorg. Chem.* **1991**, *30*, 4654.
(6) Connick, P. A.; Haller, K. J.; Macor, K. A. *Inorg. Chem.* **1993**, *32*, 3256.
(7) Kadish, K. M.; Franzen, M. M.; Han, B. C.; Araullo-McAdams, C.; Sazou, D. *J. Am. Chem. Soc.* **1991**, *113*, 512.
(8) Kadish, K. M.; Franzen, M. M.; Han, B. C.; Araullo-McAdams, C.; Sazou, D. *Inorg. Chem.* **1992**, *31*, 4399.
(9) Lexa, D.; Momenteau, M.; Mispelter, J.; Savéant, J.-M. *Inorg. Chem.* **1989**, *28*, 30.
(10) Chang, D.; Malinski, T.; Ulman, A.; Kadish, K. M. *Inorg. Chem.* **1984**, *23*, 817.

Table 2. Half-Wave Potentials ($E_{1/2}$, V vs SCE) for Reduction or Oxidation of the Investigated Nickel Porphyrins in CH_2Cl_2 Containing 0.1 M TBAP or 0.1 M $TBAPF_6$

	TBAP				$TBAPF_6$				$TBAPF_6$ − TBAP		
compd	Red(1)	Ox(1)	Ox(2)	$\Delta\lvert Ox_2 - Ox_1\rvert$	Red(1)	Ox(1)	Ox(2)	$\Delta\lvert Ox_2 - Ox_1\rvert$	ΔRed(1)	ΔOx(1)	ΔOx(2)
TPP[1,10]	−1.28	1.05	1.17	0.12	−1.31	1.01	1.31	0.30	−0.03	−0.04	+0.14
T(4-Cl-P)P[1,10]	−1.18	1.13	1.13	0.00	−1.26	1.10	1.34	0.24	−0.08	−0.03	+0.21
T(4-Et_2N-P)P[1,10]	−1.36	0.62	0.97	0.35	−1.43	0.58	1.01	0.43	−0.07	−0.04	+0.04
F_{20}TPP	−0.85	1.41	1.41	0.00	−0.90	1.42	1.67	0.25	−0.05	+0.01	+0.26
T(^{t}Bu)P	−1.48	0.60	0.93	0.33	−1.50	0.64	0.93	0.29	−0.02	+0.04	0.00
T(C_3F_7)P	−0.72	1.54	1.54	0.00	−0.73	1.54	1.67	0.13	−0.01	0.00	+0.13
T(^{i}Pr)P	−1.44	0.81	1.18	0.37	−1.46	0.83	1.20	0.37	−0.02	+0.02	+0.02
T(Me)P[1,10]	−1.36	0.83	1.15	0.32	−1.40	0.80	1.26	0.46	−0.04	−0.03	+0.11
T(Et)P[1,10]	−1.39	0.85	1.15	0.30	−1.45	0.81	1.26	0.45	−0.06	−0.04	+0.11
T(Pr)P[1,10]	−1.41	0.85	1.15	0.30	−1.45	0.81	1.26	0.45	−0.04	−0.04	+0.11
T(Bz)OEP	−1.23	0.94	1.20	0.26	−1.24	0.93	1.21	0.28	−0.01	−0.01	+0.01
OET(3-Th)P	−1.59	0.68	0.89	0.21	−1.60	0.67	1.00	0.33	−0.01	−0.01	+0.11
OETPP[67]	b	0.63	0.90	0.27	b	0.54	0.90	0.36	c	−0.09	0.00
OETNP	−0.64[a]	1.41	d	e	−0.48[a]	1.54	d	e	c	+0.13	e
F_{20}OETPP	−1.19	d	d	e	−1.19	1.04	1.44	0.40	0.00	e	e
TC6TPP	−1.56	0.66	0.98	0.32	b	d	d	e	c	e	e
Br_8TPP	−0.80	1.20	1.20	0.00	−0.87[a]	1.25	1.25	0.00	c	+0.05	+0.05
Br_8F_{20}TPP	−0.42	1.50	1.50	0.00	−0.43	1.66	1.66	0.00	−0.01	+0.16	+0.16
DPP	−1.37	0.75	0.83	0.08	−1.42	0.71	1.01	0.30	−0.05	−0.04	+0.18
F_4DPP	−1.30	0.86	0.86	0.00	−1.34	0.81	1.06	0.25	−0.04	−0.05	+0.20
F_8DPP	−1.26	0.85	0.85	0.00	−1.30	0.84	1.04	0.20	−0.04	−0.01	+0.19
F_{12}DPP	−1.17	0.89	0.89	0.00	−1.24	0.88	1.08	0.20	−0.07	−0.01	+0.19
$(OMe)_{20}$DPP	−1.38	0.75	0.87	0.12	−1.38	0.73	0.91	0.18	0.00	−0.02	+0.04
OPT(3-Th)P	−1.35	0.81	0.81	0.00	b	d	d	e	c	e	e
F_8DPP (meso)	−1.19	1.02	1.16	0.14	−1.26	0.96	1.34	0.38	−0.07	−0.06	+0.18
F_{20}DPP	−0.92	1.25	1.25	0.00	−0.96	1.30	1.52	0.22	−0.04	+0.05	+0.27
F_{28}DPP	−0.80	1.31	1.31	0.00	−0.82	1.38	1.57	0.19	−0.02	+0.07	+0.26
F_{36}DPP	d	a	d	e	−0.60	1.58	1.58	0.00	c	e	e
T(4-NO_2-P)OPP	−1.13[a]	0.98	0.98	0.00	b	0.98	1.16	0.18	c	0.00	0.18

[a] E_{pc} at 0.1 V/s. [b] $E_{1/2}$ values were not measured. [c] Not calculated because reductions have not been studied with both supporting electrolytes or because reductions are not reversible or are only reversible with one type of supporting electrolyte. [d] Value was not measured or process was not observed. [e] Could not be calculated because Ox(2) or Ox(1) values were not available.

Table 3. UV−Visible and ESR Data (λ_{max} and $\epsilon \times 10^{-4}$ $m^{-1}\cdot cm^{-1}$) of Neutral, Oxidized, and Reduced (P)Ni^{II} Derivatives in CH_2Cl_2 Containing 0.2 M $TBAPF_6$ or 0.2M TBAP

	neutral				ESR		reduced			oxidized		
macrocycle (P)	*B*(0,0)	*Q*(1,0) (II)	*Q*(0,0) (I)	I/II	Δ*H*	g	first			first		second
TPP[10]	414 (19.1)	525 (3.7)	555 (sh)[a]				414	522	600	410	606	350
T(4-Cl-P)P[10]	416 (19.8)	527 (2.5)	558 (sh)[a]				416	612	748	410	649	352
T(4-Et_2N-P)P[10]	447 (16.8)	542 (3.0)	587 (2.6)	0.87			442	545	607	406	492	416
T(C_3F_7)P	406 (9.54)	548 (0.6)	588 (1.7)	2.83								
T(^{i}Pr)P	424 (7.2)	549 (0.6)	583 (0.1)	0.18	11.0	2.007						
T(Me)P[10]	418 (18.9)	537 (1.2)	570 (sh)[a]				418	600	722	431	558	422
T(Et)P	417 (18.6)	535 (1.1)	572 (sh)[a]				417	601	723	434	560	423
T(Bz)OEP	424 (28.9)	543 (2.2)	583 (0.7)	0.32	10.8	2.007						
OET(3-Th)P	433 (14.3)	552 (0.9)	588 (0.7)	0.81	24.1	1.998						
TC6TPP	415 (7.0)	542 (0.4)	578 (0.5)	1.17	12.0	2.001						
DPP	450 (17.0)	567 (1.7)	611 (1.8)	1.06			484	713	427	748	353	
F_4DPP	447 (16.9)	565 (1.3)	611 (1.4)	1.05	6.00	2.007	486	727	429	745	352	
F_8DPP	447 (18.8)	566 (1.7)	611 (1.8)	1.01	5.20	2.007	489	725	429	743	357	
F_{12}DPP	446 (14.3)	566 (1.3)	609 (1.3)	1.01			486	723	428	739	354	
$(OMe)_{20}$DPP	455 (14.0)	569 (1.5)	613 (1.8)	1.20			b	b	b	412	747	361
(F_8DPP)(meso)	436 (20.6)	559 (1.8)	599 (2.2)	1.22			486	676	976	406	715	368
F_{20}DPP	434 (18.5)	557 (1.6)	595 (2.4)	1.55	12.0	2.008	467	656	944	409	702	339
F_{28}DPP	433 (19.0)	556 (1.9)	597 (2.7)	1.42			462	652	941	409	705	327

[a] Shoulder peak. [b] Irreversible chemical reaction.

phyrins, obtained in dichloromethane containing 0.1 M TBAP or 0.1 M $TBAPF_6$ as the supporting electrolyte, are presented in Table 2. Spectroscopic data were obtained for a selected group of the neutral, reduced, and oxidized forms of the electrochemically examined nickel porphyrins (Table 3) and confirmed that in all cases it was the porphyrin macrocycle and not the nickel atom that was oxidized or reduced under the conditions of our electrochemical experiments, i.e., in CH_2Cl_2 solutions containing 0.1 M TBAP or 0.1 M $TBAPF_6$. For example, Figure S1 of the Supporting Information shows the EPR spectrum of the species generated upon oxidation of (F_{20}DPP)Ni; the *g* value of 2.008 is consistent with the formation of a π-cation radical rather than a nickel(III) species.

The potentials for the first reversible reduction of the 29 compounds at the porphyrin macrocycle to give a π-anion radical are listed as Red(1) in Table 2. The potentials vary significantly as a function of the peripheral substituents, with

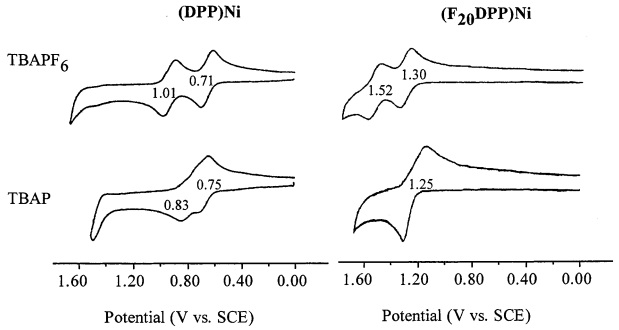

Figure 2. Effect of supporting electrolyte on electrochemical behavior of (DPP)Ni and (F_{20}DPP)Ni. All cyclic voltammograms were recorded at a scan rate of 0.1 V/s.

$E_{1/2}$ values ranging from −0.42 V in the case of (Br_8F_{20}-TPP)Ni (**18**) to −1.60 V in the case of (OET(3-Th)P)Ni (**12**). The difference between the first reduction potentials in 0.1 M TBAP or 0.1 M $TBAPF_6$, ΔRed(1), is also listed in Table 2. The values of ΔRed(1) are small, indicating that there is little effect of the supporting electrolyte on $E_{1/2}$ for the first reduction.

The range of $E_{1/2}$ values for the first oxidation to give a Ni(II) π-cation radical is also large. These values are listed as Ox(1) in Table 2 and vary from +0.54 V in the case of (OETPP)Ni (**13**) to +1.66 V in the case of (Br_8F_{20}TPP)Ni (**18**). For several compounds, the effect of the supporting electrolyte on the first macrocycle oxidation, ΔOx(1), is larger than when the macrocycle is reduced, although in a majority of cases the values of ΔOx(1) are again small and of the same magnitude as ΔRed(1). This indicates only a small effect of the type of supporting electrolyte on $E_{1/2}$ for the first oxidation. The relationship between the first macrocycle oxidation and first macrocycle reduction potentials and the electronic properties of the porphyrin substituents are discussed in more detail in Section III.

The potential for the second macrocycle oxidation, Ox(2), which gives the Ni(II) π-dication, is significantly affected by the type of supporting electrolyte, in contrast to the first macrocycle oxidation potential which showed little dependence on the supporting electrolyte. Values of ΔOx(2), the difference in the $E_{1/2}$ values for the second oxidation of the same compound using 0.1 M TBAP or 0.1 M $TBAPF_6$ as the supporting electrolyte, are given in Table 2. Changing from TBAP to $TBAPF_6$ typically results in a positive shift in Ox(2) which can be as large as 270 mV.

The absolute values of the separations between the first and second oxidations measured with the same supporting electrolyte, $\Delta|Ox_2 - Ox_1|$, are summarized in Table 2 for each examined nickel porphyrin. The experimentally measured values of $\Delta|Ox_2 - Ox_1|$ range from 0 mV (i.e., two overlapping oxidations) to 460 mV depending upon the porphyrin macrocycle and the supporting electrolyte. The electronic and structural factors influencing $\Delta|Ox_2 - Ox_1|$ are also analyzed in more detail in section III.

Two illustrations of how the supporting electrolyte affects the oxidation potentials are provided in Figure 2 for the compounds (DPP)Ni and (F_{20}DPP)Ni. As seen in this figure, the first two oxidations of (DPP)Ni (**19**) are separated by 300 mV in dichloromethane containing 0.1 M $TBAPF_6$ but by only 80 mV in dichloromethane containing 0.1 M TBAP. The first oxidation shifts positively by 40 mV upon going from $TBAPF_6$ to TBAP while the second oxidation shifts negatively by 180 mV, thus resulting in two partially overlapped processes with a $\Delta|Ox_2 - Ox_1|$ value of 80 mV. The two oxidations are more completely overlapped for the case of (F_{20}DPP)Ni (**26**) in TBAP ($\Delta|Ox_2 - Ox_1| = 0.0$ V) as compared to oxidation of the same compound in solutions of $TBAPF_6$ where the separation between the two oxidations is 220 mV.

Table 4. Assignments of Macrocycle Conformations and π-Cation Radicals for Nickel Porphyrins **1**−**29**[a]

macrocycle (P)	π-cation radical	conformation
TPP	$\mathbf{a_{2u}}$[64−67]	**planar**[16−18]
T(4-Cl-P)P	a_{2u}	*planar* (by analogy with **1**)
T(4-Et_2N-P)P	a_{2u}	*planar* (by analogy with **1**)
F_{20}TPP	a_{1u}	*planar* (by analogy with **1**)
T(^{t}Bu)P	$\mathbf{a_{1u}/a_{2u}}$[68]	**ruffled**[21,39]
T(C_3F_7)P	a_{1u}	**ruffled** (X-ray and MM this work)
T(^{i}Pr)P	a_{2u}	**ruffled**[21,23]
T(Me)P	a_{2u}	**planar**[19−21]
T(Et)P	a_{2u}	**planar**[21]
T(Pr)P	a_{2u}	**planar**[21]
T(Bz)OEP	a_{1u}	**ruffled** (X-ray and MM this work)
OET(3-Th)P	a_{1u}	*saddled* (by analogy with **13**, **15**, **16**)
OETPP	$\mathbf{a_{1u}}$[67]	**saddled**[14,34]
OETNP	a_{1u}	**mixed**[37,38]
F_{20}OETPP	a_{1u}	**saddled** (X-ray and MM this work)
TC6TPP	a_{1u}	**saddled**[14,34]
Br_8TPP	$\mathbf{a_{2u}}$[61]	*saddled* (by analogy with **18**)
Br_8F_{20}TPP	a_{1u}	**saddled**[41]
DPP	$\mathbf{a_{2u}}$[47]	**mixed**[40,46,47]
F_4DPP	a_{2u}	**mixed** (MM this work)
F_8DPP	a_{2u}	**mixed** (MM this work)
F_{12}DPP	a_{2u}	**mixed** (MM this work)
$(OMe)_{20}$DPP	a_{2u}	*mixed* (by analogy with other D(Ar)P)
OPT(3-Th)P	a_{2u}	*mixed* (by analogy with other D(Ar)P)
F_8DPP (meso)	a_{1u}	**mixed** (MM this work)
F_{20}DPP	a_{1u}	**mixed**[46] (MM this work)
F_{28}DPP	a_{1u}	**mixed** (MM this work)
F_{36}DPP	a_{1u}	**mixed** (MM this work)
T(4-NO_2-P)OPP	a_{1u}	*mixed* (by analogy with other D(Ar)P)

[a] Conformations in bold were assigned on the basis of X-ray or molecular mechanics (MM) structures. Conformations in italics are those proposed by analogy with related compounds in the same group. Radical assignments in bold were taken from the literature. Other radical assignments are those proposed in the text.

II. Structural Studies. Previous studies[1,11−13] have indicated that the substituents affect the redox behavior of the porphyrin ring via direct electronic effects and by nonplanar deformations of the macrocycle induced by crowding at the porphyrin periphery. To aid in understanding the influence of structural effects on the electrochemical behavior of porphyrins **1**−**29**, the conformations of the porphyrins were analyzed using X-ray crystallography and molecular mechanics (MM) calculations. Table 4 gives an overview of the structural characteristics (planar, saddled or ruffled or mixed (saddled and/or ruffled) of nickel porphyrins **1**−**29**, Table 5 provides more detailed structural data for some of

(11) Ravikanth, M.; Chandrashekar, T. K. *Struct. Bonding (Berlin)* **1995**, *82*, 105.
(12) Shelnutt, J. A.; Song, X.-Z.; Ma, J.-G.; Jia, S.-L.; Jentzen, W.; Medforth, C. J. *Chem. Soc. Rev.* **1998**, *27*, 31.
(13) Senge, M. O. In *The Porphyrin Handbook*; Kadish, K. M., Smith, K. M., Guilard, R., Eds.; Academic Press: Boston, 2000; Vol. 1, p 239.

Table 5. Selected X-ray Crystallographic Data for Nickel Porphyrins

porphyrin	Ni−N[a] (Å)	ϕ_{pyr}[b] (deg)	ΔC_β[c] (Å)	ΔC_m[d] (Å)	$\Delta 24$[e] (Å)	ref
"planar"						
(TPP)Ni	1.931	14.4	0.18	0.45	0.22	16
(T(Me)P)Ni	1.943	3.3	0.08	0.07	0.07	19,20
(OEP)Ni (triclinic A)	1.958	1.7	0.06	0.03	0.02	85
(OEP)Ni (tetragonal)	1.929	16.4	0.27	0.51	0.26	86
"saddled"						
(OETPP)Ni	1.906	29.4	1.23	0.03	0.62	34
(F_{20}OETPP)Ni	1.901	25.8	1.15	0.05	0.59	this work
(TC6TPP)Ni	1.914	24.8	1.08	0.02	0.54	34
(Br_8F_{20}TPP)Ni,	1.898	27.9	1.16	0.19	0.61	79
"ruffled"						
(T(C_3F_7)P)Ni	1.886	27.1	0.33	0.86	0.42	this work
(T(Bz)OEP)Ni	1.885	25.7	0.31	0.79	0.39	this work
(T(^{i}Pr)P)Ni	1.896	22.8	0.27	0.74	0.36	27
(Br_8T(CF_3)P)Ni	1.88	32.0	0.38	1.06	0.50	26
(T(Bu)OEP)Ni	1.873	31.2	0.37	1.05	0.46	27
"mixed"						
(DPP)Ni	1.909	27.8	0.36	0.86	0.43	46
(DPP)Ni	1.894	29.7	0.35	0.92	0.45	47
(DPP)Ni	1.885	31	1.02	0.60	0.59	47

[a] Average nickel−nitrogen distance. [b] Average angle between the least-squares plane of the 24 atoms of the porphyrin macrocycle and the least-squares planes of the pyrrole rings. [c] Average displacement of the β carbon atoms from the least-squares plane of the 24 atoms of the porphyrin ring. [d] Average displacement of the meso carbon atoms from the least-squares plane of the 24 atoms of the porphyrin ring. [e] Average displacement of the 24 atoms of the porphyrin macrocycle from the least-squares plane of the 24 atoms of the porphyrin ring.

Table 6. Selected Crystallographic Experimental Data for Compounds **6**, **11**, and **15**[a]

	6	**11**	**15**
chemical formula	$C_{32}H_8F_{28}N_4Ni$	$(C_{64}H_{60}N_4NiO_8)\cdot(CH_2Cl_2)$	$C_{60}H_{40}F_{20}N_4Ni\cdot 4(H_2O)$
formula weight	1039.13	1156.85	1327.73
space group	*C*2/*c* (No. 15)	*C*2/*c* (No. 15)	*C*2 (No. 5)
a (Å)	21.328(4)	22.839(12)	25.945(5)
b (Å)	16.957(3)	17.915(9)	8.276(2)
c (Å)	21.573(4)	16.124(8)	14.357(3)
β (deg)	118.82(3)	122.030(9)	108.57(3)
volume (Å^3)	6836(2)	5593(5)	2922.2(10)
Z	8	4	2
λ (Å)	1.541 78	0.710 73	0.710 73
T (K)	130(2)	90(2)	130(2)
μ (mm^{-1})	2.607	0.504	0.447
D_{calcd} (g cm^{-3})	2.019	1.373	1.509
R (F_o^2) ($>2\sigma(I)$)	0.0654	0.0993	0.0630
R_w (F_o^2) (all data)	0.1715	0.2111	0.1741

[a] $R1 = \sum||F_o| - |F_c||/\sum|F_o|$ and $wR2 = [\sum[w(F_o^2 - F_c^2)^2]/\sum[w(F_o^2)^2]]^{1/2}$; $w = 1/[\sigma^2(F_o^2) + ((X)P)^2 + (Y)P]$, where $P = (F_o^2 + 2F_c^2)/3$. For **6**, $X = 0.092\,600$ and $Y = 58.846\,199$; for **11**, $X = 0.060\,500$ and $Y = 204.242\,783$; for **15**, $X = 0.083\,800$ and $Y = 3.272\,800$.

the nickel porphyrins, and Table 6 summarizes crystallographic data for the three nickel porphyrins characterized in this work. Table S1 of the Supporting Information summarizes the energies obtained for different conformations of the (D(Ar)P)Ni macrocycles **19**−**22** and **25**−**28** using MM calculations.[14,15]

X-ray and MM studies of (TPP)Ni (**1**)[16−18] and (T(alkyl)P)-Ni macrocycles with methyl (**8**), ethyl (**9**), or propyl (**10**) groups[19−21] indicate that these porphyrins typically adopt planar and/or slightly nonplanar conformations. These uncrowded porphyrins are not intrinsically very nonplanar because they lack bulky substituents or appreciable crowding of the substituents. The structures of this group of porphyrins are characterized by long Ni−N bond distances (e.g., 1.943 Å in (T(Me)P)Ni and 1.929 Å in (TPP)Ni), small out-of-plane displacements of the meso and β carbon atoms, small angles of the pyrrole rings with respect to the least-squares plane of the porphyrin ring, and small average out-of-plane displacements of the atoms of the porphyrin core ($\Delta 24$ values) (see Table 5). Some uncrowded nickel porphyrins have been shown to exist as mixtures of planar and slightly nonplanar conformations in solution,[17,22] reflecting a tradeoff between the requirement of the porphyrin to maintain a planar

(14) Shelnutt, J. A.; Medforth, C. J.; Berber, M. D.; Barkigia, K. M.; Smith, K. M. *J. Am. Chem. Soc.* **1991**, *113*, 4077.
(15) Song, X.-Z.; Jaquinod, L.; Jentzen, W.; Nurco, D. J.; Jia, S.-L.; Khoury, R.; Ma, J.-G.; Medforth, C. J.; Smith, K. M.; Shelnutt, J. A. *Inorg. Chem.* **1998**, *37*, 2009.
(16) Maclean, A. L.; Foran, G. J.; Kennedy, B. J.; Turner, P.; Hambley, T. W. *Aust. J. Chem.* **1996**, *49*, 1273.
(17) Jentzen, W.; Unger, E.; Song, X. Z.; Jia, S. L.; TurowskaTyrk, I.; Schweitzer-Stenner, R.; Dreybrodt, W.; Scheidt, W. R.; Shelnutt, J. A. *J. Phys. Chem. A* **1997**, *101*, 5789.
(18) Rush, T. S.; Kozlowski, P. M.; Piffat, C. A.; Kumble, R.; Zgierski, M. Z.; Spiro, T. G. *J. Phys. Chem. B* **2000**, *104*, 5020.
(19) Ulman, A.; Gallucci, J.; Fisher, D.; Ibers, J. A. *J. Am. Chem. Soc.* **1980**, *102*, 6852.
(20) Pace, L. J.; Ulman, A.; Ibers, J. A. *Inorg. Chem.* **1982**, *21*, 199.
(21) Jentzen, W.; Hobbs, J. D.; Simpson, M. C.; Taylor, K. K.; Ema, T.; Nelson, N. Y.; Medforth, C. J.; Smith, K. M.; Veyrat, M.; Mazzanti, M.; Ramasseul, R.; Marchon, J.-C.; Takeuchi, T.; Goddard, I. W. A.; Shelnutt, J. A. *J. Am. Chem. Soc.* **1995**, *117*, 11085.
(22) Alden, R. G.; Crawford, B. A.; Doolen, R.; Ondrias, M. R.; Shelnutt, J. A. *J. Am. Chem. Soc.* **1989**, *111*, 2070.

π-system and the requirement of the nickel(II) atom for a short metal−nitrogen distance; the latter forces the macrocycle into a nonplanar conformation. Molecular mechanics (MM) calculations and experimental studies confirm the presence of small energy differences between planar and nonplanar structures of β-octaalkylporphyrins and *meso*-tetraarylporphyrins.[17,22] All of the uncrowded porphyrins used in this study (**1**−**4** and **8**−**10**) are classified as planar in Table 4, signifying that they adopt planar or slightly nonplanar structures.

In the case of the tetraalkylporphyrins with larger substituents [e.g., (T(^{t}Bu)P)Ni (**5**), (T(C_3F_7)P)Ni (**6**), and (T(^{i}Pr)P)Ni (**7**)], the increased peripheral steric repulsion is expected to make the porphyrin macrocycles more nonplanar. The crystal structure[23] and MM structure[21] of (T(^{i}Pr)P)Ni are best described in terms of a moderately ruffled conformation. In the ruffled conformation, the pyrrole rings are twisted alternately clockwise or anticlockwise such that the meso positions are moved alternately above or below the least-squares plane of the porphyrin ring.[24] The average out-of-plane displacement of the meso carbon atoms is 0.74 Å, and the Ni−N distance is shortened to 1.896 Å, consistent with the core contraction that is known to occur with the ruffling deformation mode.[15]

The bulkier *tert*-butyl groups in (T(^{t}Bu)P)Ni (**5**) provide even greater steric repulsion and force the macrocycle into a strongly ruffled conformation, as evidenced by crystallographic data[25] and by the results of MM calculations.[21] Other examples of strongly ruffled macrocycles are seen for 2,3,7,8,12,13,17,18-octabromo-5,10,15,20-tetrakis(trifluoromethyl)porphinatonickel(II) [(Br_8T(CF_3)P)Ni][26] and 2,3,7,8,12,13,17,18-octaethyl-5,10,15,20-tetrabutylporphinatonickel(II) [(T(Bu)OEP)Ni],[27] where the displacements of the meso carbon atoms (approximately 1.05 Å) are much larger than those seen for (T(^{i}Pr)P)Ni (Table 5).

The crystal structure of (T(C_3F_7)P)Ni had not been determined prior to this work, and on the basis of data available for other metal complexes having this macrocycle, the structural assignment was not immediately evident. The crystal structures of the free base,[28] the zinc pyridine complex,[29] and the iron(II) bispyridine complex[30] all show porphyrin macrocycles that are moderately ruffled, with average deviations of the meso carbon atoms from the least-squares plane of the porphyrin plane (free base) or the four nitrogen atoms (Fe or Zn complex) of 0.29, 0.41, and 0.62 Å, respectively. In contrast, the crystal structure of the cobalt(II) complex showed a very nonplanar structure which was predominantly saddle distorted.[31] In the saddle conformation, the pyrrole rings are tilted alternately up or down with respect to the least-squares plane of the porphyrin ring.[24]

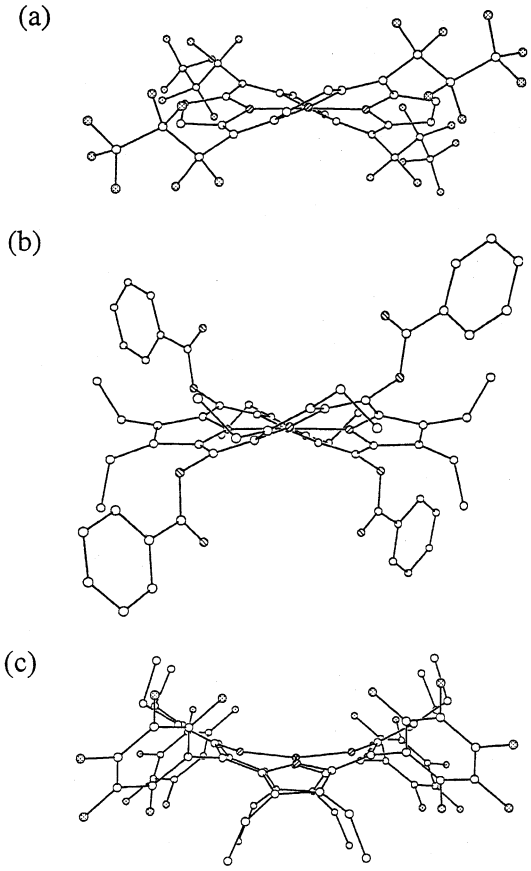

Figure 3. Side views of crystal structures of (a) (T(C_3F_7)P)Ni, (b) (T(Bz)OEP)Ni, and (c) (F_{20}OETPP)Ni illustrating the nonplanar conformations of the porphyrin macrocycles and the orientations of the peripheral substituents. Hydrogen atoms have been omitted for clarity.

The crystal structure of (T(C_3F_7)P)Ni is shown in Figure 3a. Crystallographic data for (T(C_3F_7)P)Ni are provided in Table 6, and selected structural parameters are summarized in Table 5. The crystal structure shows that (T(C_3F_7)P)Ni adopts a moderately ruffled structure, with the meso carbon atoms being displaced out of the least-squares plane of the 24 atoms of the porphyrin core by an average of 0.86 Å, the pyrrole rings being twisted by approximately 27° with respect to the porphyrin plane, and a short Ni−N distance of 1.886 Å (Table 5). The degree of ruffling is larger than that seen for the zinc(pyridine) complex[29] and the iron(II)(pyridine)$_2$ complex,[30] in agreement with the known tendency of small metal atoms to induce additional nonplanar deformation.[32] The minimum structure obtained from molecular mechanics (MM) calculations is in close agreement with the crystal structure of (T(C_3F_7)P)Ni. On the basis of the X-ray and MM data, the structures of (T(Bu)P)Ni (T(C_3F_7)P)Ni, and (T(Bu)P)-

(23) Ema, T.; Senge, M. O.; Nelson, N. Y.; Ogoshi, H.; Smith, K. M. *Angew. Chem., Int. Ed. Engl.* **1994**, *33*, 1879.
(24) Scheidt, W. R.; Lee, Y. J. *Struct. Bonding (Berlin)* **1987**, *64*, 1.
(25) Drain, C. M.; Gentemann, S.; Roberts, J. A.; Nelson, N. Y.; Medforth, C. J.; Jia, S. L.; Simpson, M. C.; Smith, K. M.; Fajer, J.; Shelnutt, J. A.; Holten, D. *J. Am. Chem. Soc.* **1998**, *120*, 3781.
(26) Nelson, N. Y.; Medforth, C. J.; Nurco, D. J.; Jia, S.-L.; Shelnutt, J. A.; Smith, K. M. *Chem. Commun.* **1999**, 2071.
(27) Senge, M. O.; Renner, M. W.; Kalisch, W. W.; Fajer, J. *J. Chem. Soc., Dalton Trans.* **2000**, 381.
(28) DiMagno, S. G.; Williams, R. A.; Therien, M. J. *J. Org. Chem.* **1994**, *59*, 6943.
(29) Goll, J. G.; Moore, K. T.; Ghosh, A.; Therien, M. J. *J. Am. Chem. Soc.* **1996**, *118*, 8344.
(30) Moore, K. T.; Fletcher, J. T.; Therien, M. J. *J. Am. Chem. Soc.* **1999**, *121*, 5196.
(31) DiMagno, S. G.; Wertsching, A. K.; Ross, C. R. *J. Am. Chem. Soc.* **1995**, *117*, 8279.
(32) Sparks, L. D.; Medforth, C. J.; Park, M.-S.; Chamberlain, J. R.; Ondrias, M. R.; Senge, M. O.; Smith, K. M.; Shelnutt, J. A. *J. Am. Chem. Soc.* **1993**, *115*, 581.

Ni are designated as ruffled in Table 4. However, we note that the T(C_3F_7)P macrocycle may exhibit some conformational flexibility, as suggested by a recent theoretical study.[33]

The other three classes of porphyrins in Table 1, T(X)OEP (**11**−**16**), Br_8T(aryl)P (**17**,**18**), and D(aryl)P (**19**−**29**), are all expected to adopt very nonplanar structures to minimize steric crowding of the peripheral substituents.[13] Compared to the nominally planar porphyrins, these macrocycles are characterized by short Ni−N bond distances (≤1.91 Å), large out-of-plane displacements of the meso or β carbon atoms, large tilt or twist angles for the pyrrole rings (25−30°), and large average out-of-plane displacements for the porphyrin atoms (0.5−0.6 Å) (Table 5).

Three of the six electrochemically investigated T(X)OEP complexes in Table 1 (**13**, **14**, and **16**) have been structurally characterized. (OETPP)Ni (**13**) and (TC6TPP)Ni (**16**) adopt saddle structures in the crystalline state.[34] Saddle conformations have also been observed for a range of other OETPP complexes.[32,35,36] In the case of (OETPP)Ni, the pyrrole rings are tilted by approximately 29° with respect to the least-squares plane of the porphyrin ring, and the β carbon atoms are on average 1.24 Å out of the porphyrin plane. (TC6TPP)Ni is slightly more planar than (OETPP)Ni (Table 5). Saddle structures are also obtained from MM calculations on OETPP(Ni) and TC6TPP(Ni).[14] An X-ray structure of (OETNP)Ni (**14**) also shows a saddle conformation.[37] However, MM calculations[38] indicate that (OETNP)Ni is conformationally flexible and that saddle, ruffle, or hybrid saddle/ruffle structures have similar energies. Accordingly, (OETNP)Ni is designated as a mixed structure while (OETPP)Ni and (TC6TPP)Ni are assigned as saddled structures in Table 4.

The structures of (T(Bz)OEP)Ni (**11**) and (F_{20}OETPP)Ni (**15**) were determined by X-ray crystallography (Table 6). As shown in Figure 3b, (T(Bz)OEP)Ni adopts a ruffled structure with only minor differences in the average out-of-plane displacement of the meso carbon atoms, the twist angle of the pyrrole ring, and the Ni−N distance compared to (T(C_3F_7)P)Ni (**6**) (Table 5). The ruffled structures seen for (T(Bz)OEP)Ni, (T(C_3F_7)P)Ni, and (T(^{t}Bu)P)Ni[39] as well as for dodecaalkylporphyrins[27,40] support the earlier suggestion[40] that the asymmetry of an sp^3 meso substituent favors a ruffled conformation.

One significant difference between the crystal structures of (T(Bz)OEP)Ni (**11**) and (T(C_3F_7)P)Ni (**6**) is the orientation of the meso substituents. In both (T(Bz)OEP)Ni and the dodecaalkylporphyrins,[27,40] the meso substituents adopt a pseudoaxial orientation in which the second carbon atom of the substituent (or the C═O group in (T(Bz)OEP)Ni)) is displaced toward the same face of the molecule as the meso carbon substituent (i.e., away from the plane of the porphyrin ring). In contrast, the perfluoroalkyl groups in (T(C_3F_7)P)Ni adopt pseudoequatorial orientations in which the second carbon atom of the substituent chain is folded back down toward the plane of the porphyrin ring.

The crystal structure of (F_{20}OETPP)Ni is illustrated in Figure 3c. The structure reveals that the porphyrin ring adopts a saddle conformation, with a large average out-of-plane displacement of the β carbon atoms (1.15 Å) and an average tilting of the pyrrole rings of approximately 26°. The structural parameters for (F_{20}OETPP)Ni are very similar to those for (OETPP)Ni.[34] MM calculations for (T(Bz)OEP)Ni and (F_{20}OETPP)Ni give minimum energy structures which are similar to those determined crystallographically. (OET(3-Th)P)Ni (**12**) is also assigned as a saddle structure by analogy with (OETPP)Ni and (F_{20}OETPP)Ni.

(Br_8F_{20}TPP)Ni has been shown by X-ray crystallography to adopt a saddle conformation.[41] Several other complexes of Br_8F_{20}TPP have also been shown to adopt saddle structures: (Br_8F_{20}TPP)Cu,[41] (Br_8F_{20}TPP)Zn,[42] and (Br_8F_{20}TPP)H_2.[43] The crystal structure of (Br_8TPP)Ni has not been determined, although both (Br_8TPP)H_2[44] and (Br_8TPP)Zn(PrCN)$_2$[45] adopt structures which are saddle distorted. Given the preponderance of data showing that Br_8T(Ar)P macrocycles favor saddle conformations, (Br_8TPP)Ni is assigned a saddle structure in Table 4.

The D(aryl)P derivatives are known to possess a greater degree of conformational flexibility than other dodecasubstituted porphyrins.[46] For example, no fewer than three crystalline forms of the parent compound (DPP)Ni have been characterized.[46,47] Crystallographic studies of (DPP)Ni and (F_{20}DPP)Ni indicate that nickel complexes of the D(aryl)P derivatives can crystallize in saddle, ruffle, or hybrid saddle/ruffle structures.[40,46,47] Molecular modeling studies are consistent with the crystallographic results as they demonstrate that ruffle and saddle conformations are the favored structures of the fluorinated D(aryl)Ps **19**−**22** and **26**−**28**. Moreover, these structures are separated by less than 4 kcal mol^{-1} (see Table S1 of the Supporting Information). On the basis of these data, all of the D(aryl)Ps were assigned as mixed structures in Table 4.

In summary, X-ray crystallography and molecular mechanics calculations can be used to divide the 29 nickel

(33) Wondimagegn, T.; Ghosh, A. *J. Phys. Chem. A* **2000**, *104*, 4606.
(34) Barkigia, K. M.; Renner, M. W.; Furenlid, L. R.; Medforth, C. J.; Smith, K. M.; Fajer, J. *J. Am. Chem. Soc.* **1993**, *115*, 3627.
(35) Barkigia, K. M.; Berber, M. D.; Fajer, J.; Medforth, C. J.; Renner, M. W.; Smith, K. M. *J. Am. Chem. Soc.* **1990**, *112*, 8851.
(36) Regev, A.; Galili, T.; Medforth, C. J.; Smith, K. M.; Barkigia, K. M.; Fajer, J.; Levanon, H. *J. Phys. Chem.* **1994**, *98*, 2520.
(37) Senge, M. O. *J. Chem. Soc., Dalton Trans.* **1993**, 3539.
(38) Hobbs, J. D.; Majumder, S. A.; Luo, L.; Sickelsmith, G. A.; Quirke, J. M. E.; Medforth, C. J.; Smith, K. M.; Shelnutt, J. A. *J. Am. Chem. Soc.* **1994**, *116*, 3261.
(39) Barkigia, K. M.; Fajer, J. Personal communication.
(40) Medforth, C. J.; Senge, M. O.; Smith, K. M.; Sparks, L. D.; Shelnutt, J. A. *J. Am. Chem. Soc.* **1992**, *114*, 9859.
(41) Henling, L. M.; Schaefer, W. P.; Hodge, J. S.; Hughes, M. E.; Gray, H. B.; Lyons, J. E.; Ellis, P. E. *Acta Crystallogr., Sect. C* **1993**, *C49*, 1743.
(42) Marsh, R. E.; Schaefer, W. P.; Hodge, J. A.; Hughes, M. E.; Gray, H. B. *Acta Crystallogr., Sect. C* **1993**, *C49*, 1339.
(43) Birnbaum, E. R.; Hodge, J. A.; Grinstaff, M. W.; Schaefer, W. P.; Henling, L.; Labinger, J. A.; Bercaw, J. E.; Gray, H. B. *Inorg. Chem.* **1995**, *34*, 3625.
(44) Bhyrappa, P.; Krishnan, V.; Nethaji, M. *Chem. Lett.* **1993**, 869.
(45) Bhyrappa, P.; Krishnan, V.; Nethaji, M. *J. Chem Soc., Dalton Trans.* **1993**, 1901.
(46) Nurco, D. J.; Medforth, C. J.; Forsyth, T. P.; Olmstead, M. M.; Smith, K. M. *J. Am. Chem. Soc.* **1996**, *118*, 10918.
(47) Barkigia, K. M.; Nurco, D. J.; Renner, M. W.; Melamed, D.; Smith, K. M.; Fajer, J. *J. Phys. Chem. B* **1998**, *102*, 322.

porphyrins into four basic structural groups: planar or nearly planar (**1**−**4**, **8**−**10**), saddled (**12**, **13**, **15**−**18**), ruffled (**5**−**7**, **11**), and mixed nonplanar (**14**, **19**−**29**). On the basis of the observed out-of-plane distortions of the β carbon atoms, the saddled porphyrins **12**, **13**, and **15**−**18** are seen to have broadly similar out-of-plane deformations, except for (TC6TPP)Ni **16** which is slightly more planar than the other porphyrins. In the case of the porphyrins with ruffled macrocycles, **6**, **7**, and **11** display similar out-of-plane displacements of the meso carbon atoms (0.80 ± 0.06 Å) but (T(Bu)P)Ni (**5**) is significantly more nonplanar.

III. Electronic and Structural Effects on Half-Wave Potentials. Previous electrochemical studies of porphyrins have demonstrated that in some cases it is possible to observe a linear relationship between $E_{1/2}$ for oxidation or reduction of the macrocycle and the substituent Hammett σ constants, whereas in other cases the electrochemical potentials cannot be reliably predicted based on the electronic properties of the substituents.[1]

Early studies of electrochemical substituent effects in para-substituted T(Ar)Ps[48−53] used the phenyl ring as the baseline aromatic system. It was shown that the oxidation or reduction potentials varied linearly with the Hammett σ parameters of the para substituents. Studies of T(Ar)P complexes with substituents at the β-pyrrole positions, where the tetraphenylporphyrin moiety was assumed to be the aromatic system being substituted, produced more varied results.[54,55] These papers also raised the question of which type of Hammett σ parameter (σ_m, σ_p, or the resonance parameters σ_p^+ or σ_p^-) should be used in the correlations. In the case of 2-substituted tetraphenylporphyrins,[54,55] a linear free energy relationship was observed with the reduction potential when the resonance parameter σ_p^- was used in the correlations. However, the best agreement between the oxidation potential and Hammett σ parameters was obtained using σ_p.[54] In addition, progressive cyanation at the pyrrole positions of tetraphenylporphyrin resulted in additive shifts in the reduction potentials but nonadditive shifts in the oxidation potentials.[54] These results were interpreted in terms of oxidation taking place at the nitrogen lone pair but reduction occurring at the porphyrin π-system. Subsequent studies also revealed marked nonadditivity in the oxidation potentials but not the reduction potentials upon progressive bromination of the pyrrole positions of T(Ar)Ps.[55−57] These and more recent studies have led to the view that it is nonplanar deformations of the porphyrin macrocycle induced by peripheral crowding which lead to the observed nonadditivity in the oxidation potentials.[1,11−13] Theoretical studies[11−13] are consistent with this view as they show that nonplanarity destabilizes the HOMO more than the LUMO.

The relationship between the half-wave potentials and the electronic properties of the substituents was analyzed for nickel porphyrins **1**−**29**. Given the diverse nature of the porphyrins in the present study, porphine (porphyrin) was used as the baseline aromatic system when examining the effect of the substituent electronic properties on the macrocycle oxidation and reduction potentials. The Hammett σ parameters for the peripheral substituents were taken from the literature[58] and are listed in Table S2 of the Supporting Information. The total electronic effect of the substituents ($\sum\sigma$) was estimated by adding the Hammett σ parameters for the substituents on the porphyrin ring. All of the commonly used Hammett σ parameters were used in attempting to find the best correlations: σ_m, σ_p, and the resonance parameters σ_p^+ (for the oxidized species) and σ_p^- (for the reduced species). Equal weight was given to the substituents at the meso and β positions when calculating $\sum\sigma$. For example, $\sum\sigma_p$ for (F_{20}DPP)Ni was calculated by summing the Hammett σ parameters for the four C_6F_5 meso substituents (4×0.27) and for the eight C_6H_5 β substituents (8×-0.01) to give a $\sum\sigma_p$ value of 1.00. Calculated sums of the substituent parameters for each of the porphyrins investigated, using either σ_m, σ_p, σ_p^+, or σ_p^-, are given in Table S3 of the Supporting Information.

Figure 4 illustrates the plots obtained for the first oxidation and first reduction versus $\sum\sigma$. Figure 4a shows the plot obtained for Ox(1) versus $\sum\sigma_p^+$ and Figure 4b the plot obtained for Red(1) versus $\sum\sigma_p^-$, both using TBAP as the supporting electrolyte. The correlation coefficient for the first macrocycle reduction process is poor for $\sum\sigma_m$ ($r = 0.787$ with 22 data points) but improves for $\sum\sigma_p$ ($r = 0.933$ with 22 data points) and is best for $\sum\sigma_p^-$ ($r = 0.940$ with 21 data points). A similar trend is seen when $TBAPF_6$ is the supporting electrolyte (see Table S4). The finding that the correlation coefficients improve with an increase in the resonance contribution to $\sum\sigma$ agrees with the results obtained from earlier studies of porphyrins containing substituents which were directly attached to the porphyrin ring.[54,55,59]

Additional plots using porphyrins categorized according to whether they had planar or nonplanar conformations did not consistently improve the correlation coefficients obtained with the reduction potentials. Full details of the different correlations are given in Table S4 of the Supporting Information. A poorer correlation ($r = 0.918$ for $\sum\sigma_p^-$) was obtained for reduction of porphyrins **1**−**3** and **8**−**10**, which have nominally planar structures. A somewhat better correlation ($r = 0.989$ for $\sum\sigma_p^-$) was obtained for porphyrins **12**, **13**, and **15**−**18**, which have saddle structures with similar degrees of nonplanar deformation (out-of-plane distortions of approximately 1.2 Å for the β carbon atoms).

(48) Kadish, K. M.; Morrison, M. M. *J. Am. Chem. Soc.* **1976**, *98*, 3326.
(49) Walker, F. A.; Beroiz, D.; Kadish, K. M. *J. Am. Chem. Soc.* **1976**, *98*, 3484.
(50) Kadish, K. M.; Morrison, M. M.; Constant, L. A.; Dickens, L.; Davis, D. G. *J. Am. Chem. Soc.* **1976**, *98*, 8387.
(51) Kadish, K. M.; Morrison, M. M. *Inorg. Chem.* **1976**, *15*, 980.
(52) Kadish, K. M.; Morrison, M. M. *Bioinorg. Chem.* **1977**, *7*, 107.
(53) Kadish, K. M.; Morrison, M. M. *Bioelectrochem. Bioenerg.* **1977**, *3*, 480.
(54) Giraudeau, A.; Callot, H. J.; Gross, M. *Inorg. Chem.* **1979**, *18*, 201.
(55) Giraudeau, A.; Callot, H. J.; Jordan, J.; Ezhar, I.; Gross, M. *J. Am. Chem. Soc.* **1979**, *101*, 3857.
(56) Ochsenbein, P.; Akoyougou, K.; Mandon, D.; Fischer, J.; Weiss, R.; Austin, R. N.; Jayarag, K.; Gold, A.; Terner, J.; Fajer, J. *J. Angew. Chem., Int. Ed. Engl.* **1994**, *33*, 348.
(57) D'Souza, F.; Zandler, M. E.; Tagliatesta, P.; Ou, Z.; Shao, J.; Van Caemelbecke, E.; Kadish, K. M. *Inorg. Chem.* **1998**, *37*, 4567.
(58) Hansch, C.; Leo, A.; Taft, R. W. *Chem. Rev.* **1991**, *91*, 165.
(59) Wu, G.-Z.; Leung, H.-K.; Gan, W.-X. *Tetrahedron* **1990**, *46*, 3233.

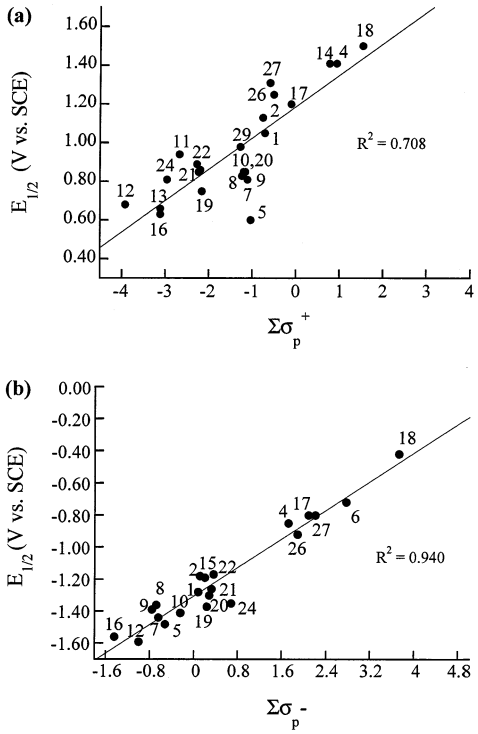

Figure 4. Plots of (a) $E_{1/2}$ for oxidation versus $\sum\sigma_p^+$ and (b) $E_{1/2}$ for reduction versus $\sum\sigma_p^-$ for nickel porphyrins. Values of $E_{1/2}$ were measured in CH_2Cl_2 containing 0.1 M TBAP.

Poor correlation coefficients ($r \leq 0.796$) were obtained in the case of the first macrocycle oxidation Ox(1) irrespective of the Hammett parameters used in the plots. Differentiating the porphyrins into planar and nonplanar systems did improve the correlation coefficients, although the best agreement between $E_{1/2}$ and $\sum\sigma$ was not necessarily obtained with the resonance Hammett σ parameters. For example, in the case of the planar porphyrins **1**−**3** and **8**−**10**, the correlation coefficient was 0.978 with $\sum\sigma_p$ but only 0.905 for $\sum\sigma_p^+$. For porphyrins **12**, **13**, and **15**−**18**, which have saddle structures with similar amounts of nonplanar distortion, the correlation coefficients were 0.992 for $\sum\sigma_p$ and 0.968 for $\sum\sigma_p^+$. We note that in the case of 2-substituted tetraphenylporphyrins[54,55] the oxidation potentials also correlated better with σ_p whereas the reduction potentials were more closely correlated with the resonance parameter σ_p^-.

$E_{1/2}$ for the first reduction of the nickel porphyrins is a reasonable indicator of the electronic effect of the peripheral substituents, as evidenced by the approximately linear correlation obtained between $E_{1/2}$ and $\sum\sigma_p^-$ for the large set of nickel porphyrins used in this study (Figure 4b). The data also indicate that a straightforward model involving equal weighting of the meso and β substituents adequately describes the electronic effect of the substituents. In the case of macrocycle oxidation, the electronic effect of the substituents is not the only factor contributing to the observed half-wave potentials, as demonstrated by the poor correlation in Figure 4a. The structural effects of the substituents (i.e., nonplanar deformations of the porphyrin macrocycle) must also be taken into account, and only for porphyrins with similar conformations (e.g., planar or saddle) are approximately linear correlations obtained with $E_{1/2}$ for oxidation. Overall, the plots obtained with a large number of nickel porphyrins support the prevailing view[1,11−13] that structural (nonplanarity) effects are more significant in determining the half-wave potential for the first macrocycle oxidation to give the π-cation radical than for the first macrocycle reduction to give the π-anion radical.

The second macrocycle oxidation of nickel porphyrins **1**−**29** to give the porphyrin dication shows a more significant dependence on the type of supporting electrolyte, as shown by the larger values of ΔOx(2) in Table 2. The difference in half-wave potentials between the first and second oxidations, $\Delta|Ox_2 - Ox_1|$, also varies considerably as a function of the porphyrin substituents and the type of supporting electrolyte (Table 2), and in some cases the two oxidations overlap. Two prior studies have examined the mechanism by which the relatively uncommon process of overlap of the oxidation reactions in porphyrins might occur.[60,61] A disproportionation reaction of the π-cation radical was proposed to account for the overlapped oxidations in the very nonplanar porphyrins $(Me_8F_{20}TPP)Zn$, $(Br_8F_{20}TPP)Zn$, and $(Cl_8F_{20}TPP)Zn$.[60] Specifically, saddling of the macrocycle in these highly substituted porphyrins was suggested to result in a_{1u} π-cation radicals which were unstable and tended to disproportionate. In a more recent study, it was speculated that the instability of the π-cation radicals was related to the near degeneracy of the a_{1u} and a_{2u} HOMOs.[61] It was proposed that a more pronounced pseudo-Jahn−Teller distortion in the dication versus the π-cation radical might favor the disproportionation reaction.

The electrochemical and structural data for nickel porphyrins **1**−**29** was used to investigate the factors controlling $\Delta|Ox_2 - Ox_1|$. Figure 5 shows plots of $\Delta|Ox_2 - Ox_1|$ versus $E_{1/2}$ for the first macrocycle reduction (which was shown in Figure 4b to be an approximate measure of the electronic effect of the peripheral substituents). The data in Figure 5a are for oxidation potentials in CH_2Cl_2 containing TBAP as supporting electrolyte and in Figure 5b are for oxidation potentials in CH_2Cl_2 containing $TBAPF_6$. Neither plot includes all of the 29 compounds, since only reversible electrode reactions were analyzed and a reversible reaction was not always observed. However, more than 20 sets of potentials are used in each plot. As shown in Figure 5b, only 2 of the 23 Ni(II) derivatives, $(Br_8F_{20}TPP)Ni$ (**18**) and (F_{36}-DPP)Ni (**28**), exhibit a $\Delta|Ox_2 - Ox_1|$ of 0.00 V in CH_2Cl_2 containing $TBAPF_6$ (compound **17** also has a 0.00 V gap but is not utilized in the plot because the first reduction of this porphyrin is not reversible). This contrasts with the results obtained in CH_2Cl_2 containing TBAP shown in Figure 5a, where 11 of the 23 investigated compounds (**2**, **4**, **6**, **18**, **20**, **21**, **22**, **24**, **26**, and **27**) are characterized by overlapped oxidations with $\Delta|Ox_2 - Ox_1| = 0.00$ V.

The general trend seen in Figure 5 is that the nickel porphyrins with more positive reduction potentials (i.e., more electron-deficient macrocycles) or with TBAP as the elec-

(60) Hodge, J. A.; Hill, M. G.; Gray, H. B. *Inorg. Chem.* **1995**, *34*, 809.
(61) Ghosh, A.; Halvorsen, I.; Nilsen, H. J.; Steene, E.; Wondimagegn, T.; Lie, R.; van Caemelbecke, E.; Guo, N.; Ou, Z.; Kadish, K. M. *J. Phys. Chem. B* **2001**, *105*, 8120.

Scheme 1

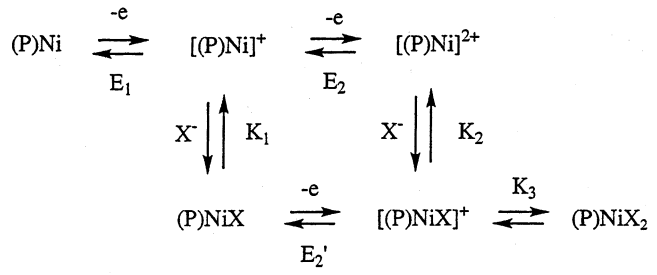

$$K_1: \quad [(P)Ni]^+ + X^- \rightleftharpoons (P)NiX \qquad K_1 = [(P)NiX] / ([X^-]\,[[(P)Ni]^+]) \qquad (1)$$

$$K_2: \quad [(P)Ni]^{2+} + X^- \rightleftharpoons [(P)NiX]^+ \qquad K_2 = [[(P)NiX]^+] / ([X^-]\,[[(P)Ni]^{2+}]) \qquad (2)$$

$$K_3: \quad [(P)NiX]^+ + X^- \rightleftharpoons (P)NiX_2 \qquad K_3 = [(P)NiX_2] / ([X^-]\,[[(P)NiX]^+]) \qquad (3)$$

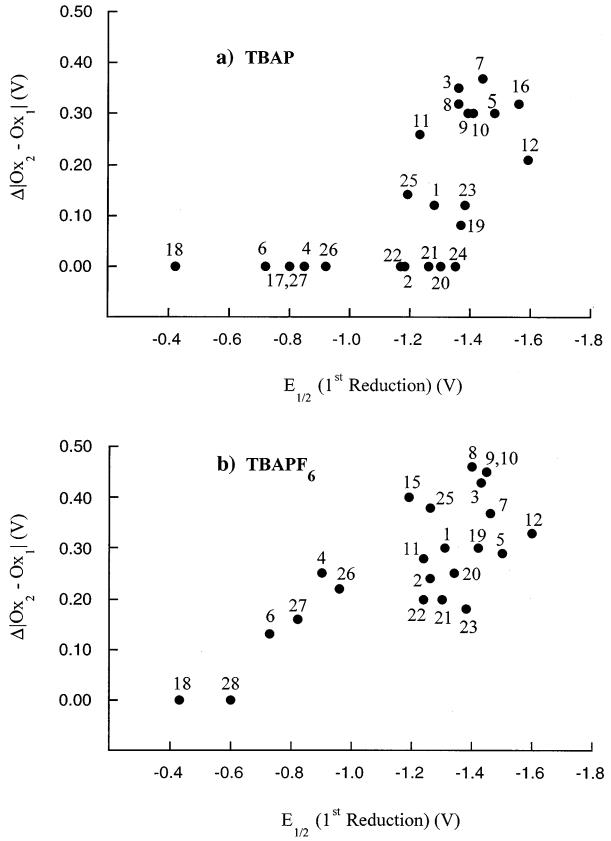

Figure 5. Plots of $\Delta|Ox_2 - Ox_1|$ versus $E_{1/2}$ for reduction in (a) dichloromethane containing 0.1 M TBAP and (b) dichloromethane containing 0.1M $TBAPF_6$.

trolyte exhibit smaller values of $\Delta|Ox_2 - Ox_1|$. This is consistent with the idea[1] that the overlap of the macrocycle-centered oxidation potentials in the nickel porphyrins is in reality related to binding of the supporting electrolyte to the dication. Anion binding effectively stabilizes the dication with respect to the π-cation radical, as shown in the mechanism illustrated in Scheme 1 (where X = ClO_4^- or PF_6^- from the supporting electrolyte). The ability of the anion from the supporting electrolyte to bind to oxidized porphyrins and stabilize higher oxidation states is well-known in the literature.[62,63]

In the presence of a weakly coordinating anion such as PF_6^-, the oxidation of (P)Ni to $[(P)Ni]^{2+}$ will occur in two separated one-electron-transfer steps labeled as E_1 and E_2 in Scheme 1. The potential E_2 will clearly be more positive than potential E_1. However, as the binding strength of $[(P)Ni]^+$ and $[(P)Ni]^{2+}$ with the anion of the supporting electrolyte increases, both oxidation potentials should be shifted in a negative direction, with the magnitude of the shift in $E_{1/2}$ depending upon the formation constants of anion binding as shown by eqs 1−3. The magnitude of K_1 is not large even in the case of ClO_4^-, since there is very little positive shift in $E_{1/2}$ for the first oxidation upon going from PF_6^- to ClO_4^- as the anion of the electrolyte. This is apparent from the small values of $\Delta Ox(1)$ seen in Table 2. In contrast, the much larger values for $\Delta Ox(2)$ in Table 2 are indicative of much stronger binding of ClO_4^- to $[(P)Ni]^{2+}$ and $[(P)NiX]^+$. This results in a negative shift of the second oxidation potential leading to a smaller value of $\Delta|Ox_2 - Ox_1|$. For example, for (F_{20}DPP)Ni (**26**) in Figure 2 and Table 2 the first oxidation shifts negatively by 50 mV upon going from $TBAPF_6$ to TBAP while the second shifts negatively by 270 mV. This is consistent with a much larger binding constant (K_2K_3) for coordination of the anion to $[(P)Ni]^{2+}$ than for anion binding to $[(P)Ni]^+$ (K_1). The stabilization of the second oxidation product by ClO_4^- appears to be so strong in the case of some compounds (**2**, **4**, **6**, **17**, **18**, **20**, **21**, **22**, **24**, **26**, and **27**) that an immediate second oxidation occurs upon formation of the monocation, thus giving what appears to be an overall two-electron transfer, i.e., the conversion of (P)Ni to $(P)NiX_2$ after the abstraction of two electrons. In this regard, it should be noted that the formal potentials given by E_1 and E_2 in Scheme 1 do not change when anion binding occurs but the actual observed reaction is easier (occurs at more negative potentials) due to the fact that the product is removed from solution by coordination.

Interestingly, there is considerable scatter in the data in Figure 5 implying that factors other than simply the electron-withdrawing or electron-donating ability of the substituents are involved in determining the gap between the oxidation potentials. To better understand these factors, the variation

(62) Seely, G. R.; Gust, D.; Moore, T. A.; Moore, A. L. *J. Phys. Chem.* **1994**, *98*, 10659.
(63) Truxillo, L. A.; Davis, D. G. *Anal. Chem.* **1975**, *47*, 2260.

in $\Delta|Ox_2 - Ox_1|$ with Red(1) was analyzed further using two available factors: (a) the conformation of the porphyrin macrocycle (planar or nonplanar, as discussed earlier and summarized in Table 4) and (b) the type of radical (a_{1u} or a_{2u}) formed when the macrocycle was oxidized. The assignments proposed for the π-cation radicals of the nickel porphyrins (Table 4) were based on a limited number of earlier assignments, optical and ESR data for the nickel porphyrins (Tables 3 and 4), and the known abilities of electron-withdrawing or electron-donating substituents at the meso or β positions of the macrocycle to stabilize or destabilize a_{1u} or a_{2u} type radicals.

T(aryl)P and T(alkyl)P porphyrins are typically expected to form a_{2u} π-cation radicals upon oxidation.[64−67] Exceptions are seen for the following compounds: (a) (T(^{t}Bu)P)Ni (**5**), which is very nonplanar and has a porphyrin π-cation radical with mixed a_{1u}/a_{2u} character);[68] (b) (T(C_3F_7)P)Ni (**6**), which likely has an a_{1u} porphyrin π-cation radical as evidenced by a *Q*(0,0) band that is more intense than the *Q*(1,0) band[60] and by the fact that the electron-withdrawing C_3F_7 substituents at the meso positions will preferentially stabilize the a_{2u} orbital; and (c) (F_{20}TPP)Ni (**24**), which is assigned as an a_{1u} radical because perfluorination of the phenyl ring switches the radical from a_{2u} in (TPP)Zn to a_{1u} in (F_{20}TPP)Zn.[69]

All the investigated T(X)OEP and Br_8T(aryl)P derivatives (see Table 1) are likely to form a_{1u} radicals upon oxidation,[32,67,70] with the exception of (Br_8TPP)Ni (**17**), which is known to form an a_{2u} π-cation radical.[61] As shown in Table 4, the radical assignments proposed for the π-cations of the D(aryl)Ps compounds are dependent upon the substituents. $[(DPP)Ni]^+$ (**19**) has been assigned as a_{2u} on the basis of its ESR spectrum.[47] As shown in Table 3, the π-cation radicals of (F_4DPP)Ni and (F_8DPP)Ni have ESR features virtually identical to that of $[(DPP)Ni]^+$, thus indicating that all three π-cation radicals are a_{2u}. In addition, the UV−visible spectra of $[(DPP)Ni]^+$, $[(F_4DPP)Ni]^+$, $[(F_8DPP)Ni]^+$, and $[(F_{12}DPP)Ni]^+$ present the same features, thus suggesting that the π-cation radical of (F_{12}DPP)Ni is also a_{2u}. Those derivatives without fluorine groups at the ortho positions of the meso phenyl rings, i.e., $[DPP(Ni)]^+$, $[(F_4DPP)Ni]^+$, $[(F_8DPP)Ni]^+$, and $[(F_{12}DPP)Ni]^+$ are thus assigned as a_{2u} radicals. The radical types of the remaining D(Ar)Ps were assigned on the basis of the electron-withdrawing ability of the aryl substituents and the optical spectra of the oxidized species. $[(F_8DPP(meso))Ni]^+$, $[(F_{20}DPP)Ni]^+$, $[(F_{28}DPP)Ni]^+$, and $[(F_{36}DPP)Ni]^+$ were assigned as a_{1u} based on the presence of the very electron-withdrawing aryl groups and a stronger *Q*(0,0) band than *Q*(1,0) band.[60] As shown in Table 3, this feature is also observed in the UV−visible spectra of (F_8-DPP(*meso*))Ni, (F_{20}DPP)Ni, (F_{28}DPP)Ni, and (F_{36}DPP)Ni, supporting the idea that all four derivatives possess a_{1u} HOMOs and form a_{1u} radicals. Based on the electronic characteristics of the porphyrin substituents, $[(T(4\text{-}NO_2\text{-}P)OPP)Ni]^+$ was tentatively assigned as an a_{1u} radical and $[((OMe)_{20}DPP)Ni]^+$ and $[(OPT(3\text{-}Th)P)Ni]^+$ as a_{2u} radicals.

The relationships between $\Delta|Ox_2 - Ox_1|$ and Red(1) for different groups of porphyrins in dichloromethane solutions containing 0.1 M TBAP or 0.1 M $TBAPF_6$ are shown in Figure 6. Nickel porphyrins with nonplanar macrocycles (i.e., saddle, ruffle, or mixed) and a_{2u} type π-cation radicals, nominally planar porphyrins with a_{2u} type π-cation radicals, and nonplanar macrocycles with a_{1u} type π-cation radicals are shown in separate plots. Insufficient data were available to produce a plot for planar porphyrins with a_{1u} type π-cation radicals. The plots with TBAP as the supporting electrolyte consist of two regions: one where the two oxidations of the nickel porphyrins are overlapped ($\Delta|Ox_2 - Ox_1| = 0$) independent of the potentials at which the compounds are reduced, and another where the values of $\Delta|Ox_2 - Ox_1|$ increase linearly as $E_{1/2}$ becomes more negative. This general pattern is again consistent with a model in which binding of the supporting electrolyte to the dication is important in determining $\Delta|Ox_2 - Ox_1|$. In the region where the two oxidations of the nickel porphyrins are overlapped, the substituents are very electron withdrawing and binding of the anion to the dication is strong, which lowers the potential for the second oxidation. In the region where the value of $\Delta|Ox_2 - Ox_1|$ increases linearly as $E_{1/2}$ becomes more negative, the substituents are less electron withdrawing and anion binding is correspondingly weaker. In this region, $\Delta|Ox_2 - Ox_1|$ is dependent upon the electron-withdrawing ability of the substituents (as measured by $E_{1/2}$ for macrocycle reduction), which determines the anion binding affinity. The plots obtained with $TBAPF_6$ as the supporting electrolyte contain fewer compounds in the region where the two oxidations of the nickel porphyrins are overlapped, consistent with the known tendency of PF_6^- anions to bind less strongly.[62,63]

Correlation coefficients, intercepts, and slopes for the regions where $\Delta|Ox_2 - Ox_1|$ increases linearly are summarized in Table S5 of the Supporting Information, and the intercepts are also indicated by an arrow in Figure 6. The correlation coefficients are sometimes poor, although the differences between the plots are consistent. Specifically, independent of the supporting electrolyte (and of whether a compound is included on the portion of the graph where $\Delta|Ox_2 - Ox_1| = 0$), the intercept of the two lines at $\Delta|Ox_2 - Ox_1| = 0$ occurs at a more positive reduction potential in the order nonplanar a_{1u} radicals, planar a_{2u} radicals, and nonplanar a_{2u} radicals. In other words, the plots indicate that independent of the supporting electrolyte used in the electrochemical measurements, more positive reduction potentials (i.e., more electron-withdrawing substituents) are required to overlap the two oxidations for a_{1u} vs a_{2u} type radicals of nonplanar porphyrins and for planar vs nonplanar

(64) Czernuszewicz, R. S.; Macor, K. A.; Li, X.-Y.; Kincaid, J.; Spiro, T. G. *J. Am. Chem. Soc.* **1989**, *111*, 3860.
(65) Fajer, D.; Davis, M. S. In *The Porphyrins*; Dolphin, D., Ed.; Academic Press: New York, 1979; Vol. IV, p 197.
(66) Spellane, P. J.; Gouterman, M.; Antipas, A.; Kim, S.; Liu, Y. C. *Inorg. Chem.* **1980**, *19*, 386.
(67) Sibilia, S. A.; Hu, S.; Piffat, C.; Melamed, D.; Spiro, T. G. *Inorg. Chem.* **1997**, *36*, 1013.
(68) Lin, C.-Y.; Hu, S.; Rush, T. R. I.; Spiro, T. G. *J. Am. Chem. Soc.* **1996**, *118*, 9452.
(69) Yang, S. I.; Seth, J.; Strachan, J.-P.; Gentemann, S.; Kim, D.; Holten, D.; Lindsey, J. S.; Bocian, D. F. *J. Porphyrins Phthalocyanines* **1999**, *3*, 117.
(70) Piffat, C.; Melamed, D.; Spiro, T. G. *J. Phys. Chem.* **1993**, *97*, 7441.

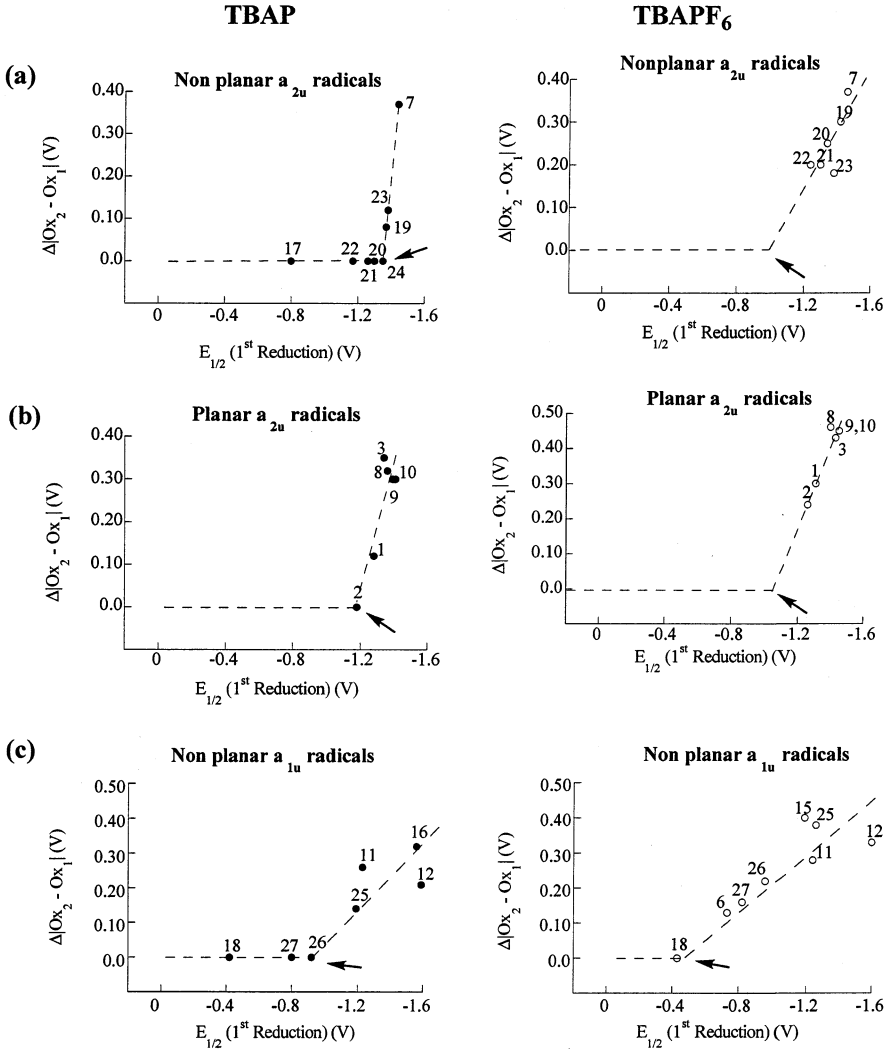

Figure 6. Plots of $\Delta|Ox_2 - Ox_1|$ versus $E_{1/2}$ for reduction in dichloromethane containing 0.1 M TBAP or 0.1 M $TBAPF_6$ for nickel porphyrins with (a) nonplanar a_{2u} radicals, (b) planar a_{2u} radicals, and (c) nonplanar a_{1u} radicals. Arrows indicate intercepts of the best regression line with the line at which $\Delta|Ox_2 - Ox_1| = 0$.

macrocycles of a_{2u} type radicals. Furthermore, for the same group of compounds (e.g., nonplanar a_{1u} radicals), more positive intercepts at $\Delta|Ox_2 - Ox_1|$ are seen for $TBAPF_6$ versus TBAP (Figure 6), consistent with weaker complexation of the perchlorate anion requiring more electron-withdrawing substituents to cause overlap of the oxidation potentials. The slopes of the regions where $\Delta|Ox_2 - Ox_1|$ increases linearly as $E_{1/2}$ becomes more negative are also clearly steeper for the nonplanar a_{2u} radicals versus the nonplanar a_{1u} radicals.

What is the significance of the dependence of the intercept on the type of radical and the porphyrin conformation, and how can these trends be explained in terms of the proposed anion binding model? Crystallographic data establish that the anions in porphyrin π-cation radicals typically bind in the vicinity of the metal atom in both nominally planar porphyrins and in very nonplanar porphyrins. For example, the distance between the metal atom and an oxygen atom of the perchlorate anion is 2.079(8) Å in $[(TPP)Zn]^+(ClO_4)$, 2.012(5) Å in $[(TPP)Mg]^+(ClO_4)$, and 2.13(1) Å in $[(TPP)Fe^{III}]^{2+}(ClO_4)_2$.[24] In $[(OETPP)Cu]^+(ClO_4)$, the copper−oxygen distance is 2.445(4) Å.[71] Assuming that the binding site of the anions is similar for the examined Ni(II) dications, an a_{2u} versus a_{1u} type radical or nonplanar versus planar conformation may generate increased positive charge on the nickel atom or allow better delocalization of any negative charge transferred from the anion. This then favors tighter anion binding and overlap of the oxidations at more negative reduction potentials (i.e., with less electron-withdrawing substituents).

It should be pointed out that if the HOMO is an a_{2u} orbital, then the HOMO-1 is an a_{1u} orbital, and that when two electrons are abstracted from the HOMO (to form a dication), the HOMO of the dication has a profile opposite that of the original HOMO; i.e., an a_{2u} cation radical will result in an a_{1u} dication and an a_{1u} cation radical will result in an a_{2u} dication. With this in mind, it is known that a_{2u} π-cation radicals have the unpaired electron spin (or the equivalent positive hole) delocalized on the meso carbon atoms and the nitrogen atoms, whereas a_{1u} π-cation radicals have the unpaired electron spin (or positive hole) delocalized on the

(71) Renner, M. W.; Barkigia, K. M.; Zhang, Y.; Medforth, C. J.; Smith, K. M.; Fajer, J. *J. Am. Chem. Soc.* **1994**, *116*, 8582.

α and β carbon atoms of the pyrrole rings.[72] Therefore, more positive potentials for overlap of the oxidations (i.e., lower anion binding affinities) may be seen for a_{1u} radicals because the a_{2u} dication derived from this radical has a filled p orbital on the nitrogen atoms and there is thus a greater π-electron density near the nickel atom. This in turn would make it more difficult to bind the anion and/or delocalize any charge transferred from the anion, thus requiring more electron-withdrawing substituents to overlap the oxidations.

The plots in Figure 6 also show that the intercepts at $\Delta|Ox_2 - Ox_1| = 0$ shift to more negative potentials for nonplanar a_{2u} radicals compared to planar a_{2u} radicals, suggesting that anion binding is stronger for the π-dications of nonplanar porphyrins. This effect appears to be weaker than the effect arising from the different types of radicals discussed above. Previous studies have shown that nonplanarity typically decreases axial amine ligand affinity,[14] in part because the substituents resist the core expansion that has to occur when the nickel atom binds axial ligands and becomes high spin. Why then does nonplanarity shift the intercepts at $\Delta|Ox_2 - Ox_1| = 0$ to more negative potentials indicative of higher anion binding affinities? One possibility is an increased interaction between the substituents and the metal center in nonplanar porphyrins versus planar porphyrins which leads to stronger anion binding in the former. In other words, the substituent effect is transmitted more strongly to the probable anion binding site (the nickel atom) when the macrocycle is nonplanar. Note that there is some precedent in the literature for such an effect; it has been shown that nonplanarity influences the interaction between the unpaired electrons on the macrocycle and the metal atom in the copper(II) complex of OETPP (**13**) by permitting the overlap of orbitals that are orthogonal in a planar porphyrin system.[71]

Overall, the plots in Figure 6 appear to be fully consistent with the idea that the dominant effect determining the gap between the macrocycle oxidation potentials in the nickel porphyrins is stabilization of the π-dication by binding of the supporting electrolyte. The magnitude of $\Delta|Ox_2 - Ox_1|$ is apparently linked to the complexing ability of the anion (which is larger for perchlorate than for hexafluorophosphate)[62,63] and the electron-withdrawing ability of the substituents (i.e., the electron density at the anion binding site). The present work also suggests that the anion binding affinity depends on other features of the macrocycle such as the type of π-cation radical and the conformation of the neutral molecule. Of note is the fact that the plots in Figure 6 still show some residual scatter even when the type of radical and the macrocycle conformation are considered. This scatter may originate from several sources such as different amounts and types of nonplanar deformation in the nonplanar porphyrins, the π-dications not possessing pure a_{1u} or a_{2u} characteristics, or electrostatic interactions between the anions and the porphyrin substituents which also affect anion binding.

In summary, the present study addresses in more detail the question of which structural and experimental features encourage overlap of the macrocycle oxidations in nickel porphyrins. Factors which are found to favor overlap of the oxidations include (a) the presence of very electron-withdrawing substituents on the porphyrin macrocycle, (b) the use of a weakly polar solvent and a strongly coordinating anion in the supporting electrolyte,[73] and (c) the formation of an a_{2u} type radical rather than an a_{1u} type radical. Nonplanar deformations of the porphyrin macrocycle also appear to favor overlap of the oxidations, although this effect is not particularly strong. Studies are currently in progress to determine if the mechanism suggested by the nickel porphyrin data also operates for other metalloporphyrins. Electrochemical data from the literature suggest that this is indeed the case.[74]

Experimental Section

Electrochemistry. Ultra-high-purity N_2 from Trigas was used to deoxygenate all solutions prior to each electrochemical experiment. Absolute dichloromethane (CH_2Cl_2) was purchased from Fluka Chemical Co. and purified as follows: It was first washed with sulfuric acid several times and stirred overnight until the yellowish color of the sulfuric acid phase disappeared. It was then washed with distilled water and dried with magnesium sulfate before being doubly distilled, first over phosphorus pentoxide (P_2O_5) and then over calcium hydride. $TBAPF_6$ and TBAP were purchased from Fluka Chemical Co. Both supporting electrolytes were recrystalized twice from absolute ethyl alcohol (TBAP) or ethyl acetate ($TBAPF_6$) and then dried in a vacuum oven at 40 °C for 3 days prior to use.

Cyclic voltammograms were obtained with an EG&G Model 173 potentiostat or 263 A potentiostat or an IBM Model EC 225 voltammetric analyzer. Current−voltage curves were recorded on an EG&G Princeton Applied Research Model RE-0151 *X*−*Y* recorder or a Zenith data system Model Z-386 SX/20 computer coupled with a Hewlett-Packard deskjet 600 plotter. A three-electrode system was used and consisted of a glassy carbon or a platinum button working electrode, a platinum wire counter electrode, and a saturated calomel reference electrode (SCE). This reference electrode was separated from the bulk solution by a fritted-glass bridge filled with the solvent/supporting electrolyte mixture. All potentials are referenced to the SCE.

X-ray Crystallography. X-ray diffraction data were collected with a Syntex $P2_1$ diffractometer with a sealed tube source [λ(Cu Kα) = 1.541 78 Å] and a locally modified LT-1 low-temperature apparatus for **6**, a Bruker SMART 1000 diffractometer with a sealed tube source [λ(Mo Kα) = 0.710 73 Å] and a Cryoindustries low-temperature apparatus for **11**, and a Siemens P3 diffractometer with a sealed tube source [λ(Mo Kα) = 0.710 73 Å] and a locally modified Nonius low-temperature apparatus for **15**. The Bruker SHELXTL V. 5.03 software package was used for structure solution and refinement; scattering factors were used as supplied. Structures were refined based on F^2 using all independent data by full matrix least-squares methods. Illustrations of the crystal structures of compounds **6**, **11**, and **15** are provided in Figure 3. A summary of experimental details is given in Table 6. Full experimental details, in CIF format, are available as Supporting Information to this article.

Molecular Mechanics Calculations. Molecular mechanics calculations were carried out using POLYGRAF software (Molec-

(72) Gouterman, M. In *The Porphyrins*; Dolphin, D., Ed.; Academic Press: New York, 1978; Vol. 3, pp 1−165.

(73) Geng, L.; Murray, R. W. *Inorg. Chem.* **1986**, *25*, 3115.

(74) Woller, E. K.; DiMagno, S. G. *J. Org. Chem.* **1997**, *62*, 1588.

ular Simulations, Inc.) and a force-field for metalloporphyrins that has been described in the literature.[14,15]

Synthesis. Electrochemical data for porphyrins **1**−**3** and **8**−**10** was taken from the literature.[10] (F_{20}TPP)Ni (**4**),[75] (T(^{t}Bu)P)Ni (**5**),[21] (T(^{i}Pr)P)Ni (**7**),[21] (OETPP)Ni (**13**),[14,35] (OETNP)Ni (**14**),[38] (TC6TPP)-Ni (**16**),[14,76] (OET(3-Th)P)Ni (**12**),[77] (Br_8TPP)Ni (**17**),[78] (Br_8F_{20}-TPP)Ni (**18**),[79] (DPP)Ni (**19**),[40] and (OPT(3-Th)P)Ni (**24**)[77] were prepared according to literature procedures. The remaining nickel porphyrins were prepared as described in the following sections. The nickel complexes were prepared by inserting nickel into the corresponding free base porphyrins using nickel acetylacetonate in refluxing xylenes or toluene. The nickel porphyrins were typically purified using column chromatography and recrystallization. ^{1}H and ^{19}F NMR spectra were measured at frequencies of 300 and 283 MHz, respectively. Spectra were typically recorded at ambient temperature (298 ± 5 K) using 2−5 mM solutions. ^{1}H chemical shifts were referenced to TMS, $CHCl_3$ at δ 7.26, $C_6D_5CHD_2$ at δ 2.09, or CD_3COCHD_2 at δ 2.05. ^{19}F chemical shifts were referenced to internal CF_2Cl_2 at −8.0 ppm.[80] Visible absorption spectra were recorded on a Hewlett-Packard 8450A spectrophotometer using CH_2Cl_2 as solvent. High-resolution FAB or EI mass spectra were obtained from the University of California, Riverside, facility. Low-resolution MALDI spectra were obtained at UC Davis as described previously.[81] Melting points (uncorrected) were measured on a Thomas/Bristoline microscopic hot stage apparatus.

5,10,15,20-Tetrakis(heptafluoropropyl)porphinato-nickel(II), (T(C_3F_7)P)Ni (6). The free base porphyrin (T(C_3F_7)P)-H_2 was prepared as described previously[28,29] and nickel inserted in 80% yield using the nickel acetylacetonate/toluene procedure. mp >300 °C. HRMS Calcd for $C_{32}H_8F_{28}N_4Ni$: 1037.966; found: 1037.965. ^{1}H NMR ($CDCl_3$): 9.32 (s, 8 H, β-H). ^{19}F NMR (CD_2-Cl_2): −120.0 (s, 8 F, $CF_2CF_2CF_3$), −86.7 (br, 8 F, $CF_2CF_2CF_3$), −81.2 (s, 12 F, CF_3). Visible spectrum (CH_2Cl_2), λ/nm (ϵ/cm^{-1} mol^{-1} dm^{-3}): 406 (95.4), 548 (6200), 588 (17 200). Anal. Calcd for $C_{32}H_8F_{28}N_4Ni$: C, 36.99; H, 0.78; N, 5.39. Found: C, 37.21, H, 0.79, N, 5.47.

5,10,15,20-Tetrabenzoate-2,3,7,8,12,13,17,18-octaethylporphinatonickel(II), (T(Bz)OEP)Ni (11). (OEP)Ni (300 mg, 0.503 mmol) was dissolved in dichloromethane (100 mL), benzoyl peroxide (0.6 g, 2.48 mmol) was added, and the mixture was stirred for 3 days at room temperature. The reaction mixture was washed with sodium carbonate and then with water, and the solvent was removed under reduced pressure. The product was purified by silica gel column chromatography using dichlromethane/cyclohexane as eluent, and recrystallized from dichlromethane/cyclohexane to afford the title compound in 45.8% yield. ^{1}H NMR ($C_6D_5CD_3$): 8.47 (m, 8H, H_{ortho}), 7.22 (m, 12H, H_{meta} and H_{para}), 3.40 and 3.61 (m, 8H each, CH_2 A and B), 1.57 (t, 24H, CH_3). Visible spectrum (CH_2-Cl_2), λ/nm (ϵ/cm^{-1} mol^{-1} dm^{-3}): 424 (289 000), 543 (22 000), 583 (7000).

2,3,7,8,12,13,17,18-Octaethyl-5,10,15,20-tetrakis(pentafluorophenyl)porphinatonickel(II), (F_{20}OETPP)Ni (15). The free base porphyrin (F_{20}OETPP)H_2 was prepared in 10.1% yield using the procedure employed in the synthesis of (OETPP)H_2.[35] ^{1}H NMR ($CDCl_3$): 3.80 and 2.18 (br, 8H each, CH_2 A and B), 0.68 (br, 24H, CH_3), −1.7 (v br, 2H, NH). ^{19}F NMR ($CDCl_3$): −137.7 (F_{ortho}), −153.0 (F_{para}), −163.2 (F_{meta}). Nickel was inserted using the nickel acetylacetonate/xylene procedure. ^{1}H NMR ($CDCl_3$): 2.42 (br, 16H, CH_2), 0.70 (t, 24H, CH_3). ^{19}F NMR ($CDCl_3$): −137.6 (F_{ortho}), −153.2 (F_{para}), −163.1 (F_{meta}). Visible spectrum (CH_2Cl_2), λ/nm (ϵ/relative intensity): 426 (1.00), 558 (0.058), 595 (0.124).

5,10,15,20-Tetrakis(4-fluorophenyl)-2,3,7,8,12,13,17,18-octaphenylporphinatonickel(II), (F_4DPP)Ni (20). The free base porphyrin was prepared as described previously[82] and nickel inserted in 83% yield using the nickel acetylacetonate/xylene procedure. mp >300 °C. ^{1}H NMR ($CDCl_3$), δ (ppm): 6.79 (t, 8H, β-H_{para}), 6.78 (t, 8H, *meso*-H_{ortho}), 6.69 (t, 16H, β-H_{meta}), 6.59 (d, 16H, β-H_{ortho}), 6.07 (t, 8H, *meso*-H_{meta}). ^{19}F NMR ($CDCl_3$): −118.8. FAB HRMS [M]$^+$ calcd 1350.3795, found 1350.3857. Visible spectrum (CH_2Cl_2), λ/nm (ϵ/cm^{-1} mol^{-1} dm^{-3}): 446 (213 000), 564 (16 200), 608 (16 700). Anal. Calcd for $C_{92}H_{56}F_4N_4Ni\cdot CH_3OH$: C, 80.70; H, 4.37; N, 4.05. Found: C, 80.86; H, 4.27; N, 4.20.

2,3,7,8,12,13,17,18-Octakis(4-fluorophenyl)-5,10,15,20-tetraphenylporphinatonickel(II), (F_8DPP)Ni (21). The free base porphyrin was prepared as described previously[82] and nickel inserted in 75% yield using the nickel acetylacetonate/xylene procedure. mp >300 °C. FAB HRMS [M]$^+$ calcd 1422.3418, found 1422.3374. ^{1}H NMR ($CDCl_3$), δ (ppm): 6.87 (d, 8H, *meso*-H_{ortho}), 6.80 (t, 4H, *meso*-H_{para}), 6.54 (t, 8H, *meso*-H_{meta}), 6.52 (t, 16H, β-H_{ortho}), 6.35 (t, 16H, β-H_{meta}). ^{19}F NMR ($CDCl_3$): −119.1. Visible spectrum (CH_2Cl_2), λ/nm (ϵ/cm^{-1} mol^{-1} dm^{-3}): 446 (200 000), 566 (15 500), 610 (15 600). Anal. Calcd for $C_{92}H_{52}F_8N_4Ni\cdot CH_3OH$: C, 76.77; H, 3.88; N, 3.85. Found: C, 77.10; H, 4.18; N, 3.78.

2,3,5,7,8,10,12,13,15,17,18,20-Dodecakis(4-fluorophenyl)porphinatonickel(II), (F_{12}DPP)Ni (22). The free base porphyrin was prepared as described previously[82] and nickel inserted in 75% yield using the nickel acetylacetonate/xylene procedure. mp >300 °C. FAB HRMS [M]$^+$ calcd 1494.3041, found 1494.3086. ^{1}H NMR ($CDCl_3$): 6.82 (q, 8H, *meso*-H_{ortho}), 6.54 (m, 16H, β-H_{ortho}), 6.45 (t, 16H, β-H_{meta}), 6.26 (t, 8H, *meso*-H_{meta}). ^{19}F NMR ($CDCl_3$): −117.9 (β-F_{para}), −116.9 (*meso*-F_{para}). Visible spectrum (CH_2Cl_2), λ/nm (ϵ/cm^{-1} mol^{-1} dm^{-3}): 446 (206 000), 564 (15 500), 608 (15 700). Anal. Calcd for $C_{92}H_{48}N_4F_{12}Ni\cdot 2(MeOH)$: C, 72.37; H, 3.62; N, 3.59. Found: C, 72.59; H, 3.47; N, 3.61.

2,3,7,8,12,13,17,18-Octakis(4-methoxyphenyl)-5,10,15,20-tetrakis(3,4,5-trimethoxyphenyl)porphinatonickel(II), ($(OMe)_{20}$DPP)-Ni (23). 3,4,5-Trimethoxybenzaldehyde (694 mg, 3.54 mmol) was dissolved in refluxing acetic acid (33 mL) and 3,4-bis(4-methoxyphenyl)pyrrole (988 mg, 3.54 mmol) dissolved in warm acetic acid (20 mL) was added to the refluxing solution. Reflux was continued for 17, h after which time DDQ (803 mg, 3.54 mmol) was added to the reaction mixture and reflux continued for another 2 h. The reaction mixture was poured into deionized water (500 mL) and extracted with dichloromethane (4 × 150 mL). The combined organic extracts were washed with deionized water (400 mL). The organic phase was shaken vigorously with aqueous 2% NaOH to convert the product to its free base form. A silica gel column (20 cm × 5 cm packed as a slurry in CH_2Cl_2) was eluted with a gradient of MeOH/CH_2Cl_2 (starting with 1% and finishing

(75) Carvalho de Medeiros, J. A.; Cosnier, S.; Deronzier, A.; Moutet, J.-C. *Inorg. Chem.* **1996**, *35*, 2659.
(76) Medforth, C. J.; Berber, M. D.; Smith, K. M.; Shelnutt, J. A. *Tetrahedron Lett.* **1990**, *31*, 3719.
(77) Medforth, C. J.; Haddad, R. E.; Muzzi, C. M.; Dooley, N. R.; Jaquinod, L.; Shyr, D. C.; Nurco, D. J.; Olmstead, M. M.; Smith, K. M.; Ma, J.-G.; Shelnutt, J. A., submitted for publication.
(78) Bhyrappa, P.; Krishnan, V. *Inorg. Chem.* **1991**, *30*, 239.
(79) Mandon, D.; Ochsenbein, P.; Fischer, J.; Weiss, R.; Jayaraj, K.; Austin, R. N.; Gold, A.; White, P. S.; Brigaud, O.; Battioni, P.; Mansuy, D. *Inorg. Chem.* **1992**, *31*, 2044.
(80) Harris, R. K.; Mann, B. E. *NMR and the Periodic Table*; Academic Press: New York, 1978.
(81) Green, M. K.; Medforth, C. J.; Muzzi, C. M.; Nurco, D. J.; Shea, K. M.; Smith, K. M.; Shelnutt, J. A.; Lebrilla, C. B. *Eur. Mass Spectrom.* **1997**, *3*, 439.
(82) Kadish, K. M.; Van Caemelbecke, E.; D'Souza, F.; Lin, M.; Nurco, D. J.; Medforth, C. J.; Forsyth, T. P.; Krattinger, B.; Smith, K. M.; Fukuzumi, S.; Nakanishi, I.; Shelnutt, J. A. *Inorg. Chem.* **1999**, *38*, 2188.

with 40% MeOH). Though free base material was loaded on the column, primarily dication was recovered in the eluate. After a basic aqueous washing and crystallization, purified ((OMe$_{20}$)DPP)H$_2$ was obtained in 58% yield (932 mg, 0.511 mmol). mp >300 °C. FAB HRMS [MH]$^+$ calcd for $C_{112}H_{103}N_4O_{20}$ 1823.7166, found 1826.7240; MALDI FT-ICR MS [MH]$^+$ 1823.7. ^{1}H NMR ($CDCl_3$): 3.63 (s, 24H, methoxyl), 3.76 (s, 12H, methoxyl), 3.79 (s, 24H, methoxyl), 6.33, 6.69 (doublets, 16H each, β-H$_{ortho}$ and β-H$_{meta}$), 6.85 (s, 8H, *meso*-H$_{ortho}$). Visible spectrum (CH_2Cl_2), λ/nm (ϵ/relative intensity): 472 (100), 562 (7.2), 612 (6.2), 718 (4.1). Visible spectrum (CH_2Cl_2 plus 1% trifluoroacetic acid), λ/nm (ϵ/relative intensity): 506 (100), 726 (26.4). The nickel complex was prepared in 91% yield using the nickel acetylacetonate/xylene procedure. mp >300 °C. FAB HRMS [M]$^+$ calcd for $C_{112}H_{100}N_4O_{20}Ni$ 1878.6284, found 1878.6211; MALDI FT-ICR MS [M]$^+$ 1878.6. ^{1}H NMR ($CDCl_3$): 6.60, 6.31 (d, 16H each, β-H$_{meta}$ and β-H$_{ortho}$), 6.22 (s, 8H, *meso*-H$_{ortho}$), 3.69 (s, 12H, *meso*-OMe$_{para}$), 3.63, 3.53 (s, 24H each, *meso*-OMe$_{meta}$ and β-OMe). Visible spectrum (CH_2Cl_2), λ/nm (ϵ/cm^{-1} mol^{-1} dm^{-3}): 452 (138 000), 568 (12 000), 612 (15 100).

5,10,15,20-Tetrakis(2,6-difluorophenyl)-2,3,7,8,12,13,17,18-octaphenylporphinatonickel(II), (F$_8$DPP)Ni (*meso) (25).* The free base porphyrin was prepared as described previously[82] and nickel inserted in 57% yield using the nickel acetylacetonate/xylene procedure. mp >300 °C. FAB HRMS [M]$^+$ calcd for $C_{92}H_{52}N_4F_8Ni$ 1422.3418, found 1422.3349. ^{1}H NMR ($CDCl_3$): 6.73 (m, 40H, β-phenyl), 6.51 (m, 4H, *meso*-H$_{para}$), 5.92 (t, 8H, *meso*-H$_{meta}$). ^{19}F NMR ($CDCl_3$): −108.4. Visible spectrum (CH_2Cl_2), λ/nm (ϵ/cm^{-1} mol^{-1} dm^{-3}): 436 (149 000), 558 (12 100), 598 (14 500).

5,10,15,20-Tetrakis(pentafluorophenyl)-2,3,7,8,12,13,17,18-octaphenylporphinatonickel(II), (F$_{20}$DPP)Ni (26). The free base porphyrin was prepared as described previously[82] and nickel inserted in 86% yield using the nickel acetylacetonate/xylene procedure. mp >300 °C. FAB HRMS [M]$^+$ calcd 1638.2287, found 1638.2270. ^{1}H NMR ($CDCl_3$): 6.95 (m, 40H, β-phenyl). ^{19}F NMR ($CDCl_3$): −166.4 (F$_{meta}$), −156.6 (F$_{para}$), −136.4 (F$_{ortho}$). Anal. Calcd for $C_{92}H_{40}F_{20}N_4Ni$: C, 67.38; H, 2.46; N, 3.42. Found: C, 67.04; H, 2.49; N, 3.35. Visible spectrum (CH_2Cl_2), λ/nm (ϵ/cm^{-1} mol^{-1} dm^{-3}): 432 (211 000), 556 (24 700), 596 (33 800).

2,3,7,8,12,13,17,18-Octakis(4-fluorophenyl)-5,10,15,20-tetrakis(pentafluorophenyl)porphinatonickel(II), (F$_{28}$DPP)Ni (27). The free base porphyrin was prepared as described previously[82] and nickel inserted in 98% yield using the nickel acetylacetonate/xylene procedure. mp >300 °C. FAB HRMS [M]$^+$ calcd 1782.1533, found 1782.1506. ^{1}H NMR ($CDCl_3$): 6.85 (m, 16H, β-H$_{ortho}$) 6.70 (t, 16H, β-H$_{meta}$). ^{19}F NMR ($CDCl_3$): −165.6 (F$_{meta}$), −154.9 (*meso*-F$_{para}$), −136.2 (F$_{ortho}$), −115.0 (β-F$_{para}$). Anal. Calcd for $C_{92}H_{32}F_{28}N_4Ni$: C, 61.94; H, 1.81; N, 3.14. Found: C, 61.94; H, 1.90; N, 3.14. Visible spectrum (CH_2Cl_2), λ/nm (ϵ/cm^{-1} mol^{-1} dm^{-3}): 432 (186 000), 556 (15 100), 596 (23 200).

2,3,7,8,12,13,17,18-Octakis(3,5-difluorophenyl)-5,10,15,20-tetrakis(pentafluorophenyl)porphinatonickel(II), (F$_{36}$DPP)Ni (28). The free base porphyrin was prepared as described previously[82] and nickel inserted in 81% yield using the nickel acetylacetonate/xylene procedure. mp >300 °C. FAB HRMS [M]$^+$ calcd for $C_{92}H_{24}N_4F_{36}Ni$ 1926.0780, found 1926.0710. ^{1}H NMR (CD_3COCD_3): 6.47 (m, 16H, β-H$_{ortho}$), 6.63 (m, 8H, β-H$_{para}$). ^{19}F NMR ($CDCl_3$): −164.4 (*meso*-F$_{meta}$), −152.6 (F$_{para}$), −135.7 (F$_{ortho}$), −110.6 (β-F$_{meta}$). Visible spectrum (CH_2Cl_2), λ/nm (ϵ/relative intensity): 434 (1.00), 557 (0.086), 595 (0.109).

5,10,15,20-Tetrakis(4-nitrophenyl)-2,3,7,8,12,13,17,18-octaphenylporphinatonickel(II), (T(4-NO$_2$-P)OPP)Ni (29). The free base porphyrin was prepared using a previously published procedure.[83,84] Nickel was inserted using the nickel acetylacetonate/xylene procedure. ^{1}H NMR ($CDCl_3$): 7.67 and 7.55 (d, 8H each, *meso*-H$_{ortho}$ and *meso*-H$_{meta}$), 6.80 (m, 8H, β-H$_{para}$), 6.66 (t, 16H, β-H$_{meta}$), 6.59 (m, 16H, β-H$_{ortho}$). Visible spectrum (CH_2Cl_2), λ/nm (ϵ/cm^{-1} mol^{-1} dm^{-3}): 450 (216 000), 566 (21 700), 612 (23 100).

Acknowledgment. The support of the Robert A. Welch Foundation (K.M.K., Grant E-680) is gratefully acknowledged. This work was supported by grants from the National Institutes of Health (HL 22252) and the National Science Foundation (CHE-99-04076) (K.M.S.). This work was partially supported by the Division of Material Sciences and Engineering, Office of Basic Energy Sciences, U.S. Department of Energy. Sandia is a multiprogram laboratory operated by Sandia Corporation, a Lockheed-Martin company, for the United States Department of Energy under Contract No. DE-ACO4-94AL85000.

Supporting Information Available: Molecular mechanics energies for (D(Ar)P)Ni complexes, Hammett σ parameters and $\sum\sigma$ values, and analyses of the plots of $E_{1/2}$ for oxidation of reduction versus $\sum\sigma$ and $\Delta|Ox_2 - Ox_1|$ versus $E_{1/2}$ for macrocycle reduction. Details of the crystal structure determinations of compounds **6**, **11**, and **15** (CIF). This material is available free of charge via the Internet at http://pubs.acs.org.

IC0200702

(83) Takeda, J.; Sato, M. *Inorg. Chem.* **1992**, *31*, 2877.
(84) Takeda, J.; Sato, M. *Chem. Pharm. Bull.* **1994**, *42*, 1005.
(85) Cullen, D. L.; Meyer, E. F. *J. Am. Chem. Soc.* **1974**, *96*, 2095.
(86) Meyer, E. F. *Acta Crystallogr., Sect. B* **1972**, *B28*, 2162.